The Pennsylvania State University

The Graduate School

Department of Energy and Mineral Engineering

PERMEABILITY OF COAL-BIOMASS MIXTURES FOR HIGH PRESSURE GASIFIER FEEDS

A Thesis in

Energy and Mineral Engineering

by

Rohan Belvalkar

Submitted in Partial Fulfillment
of the Requirements
for the Degree of

Master of Science

May 2012

The thesis of Rohan Belvalkar was reviewed and approved* by the following:

Derek Elsworth
Professor of Energy and Geo-Environmental Engineering
Thesis Advisor

Chris Marone
Professor of Geosciences

Jonathan Mathews
Assistant Professor of Energy and Mineral Engineering

Larry Grayson
Professor
Chair of Graduate Program of Energy and Mineral Engineering

*Signatures are on file in the Graduate School

ABSTRACT

Complete measurements of permeability on coal-biomass mixtures as a potential feedstock to gasifiers to reduce net carbon emissions were performed. Permeability is measured under anticipated dry feed stress conditions to determine the potential for fugitive gas emissions from the gasifier into the feed hopper. Cylindrical samples of coal-biomass blends are housed within a triaxial apparatus capable of applying mean and deviatoric stresses and of concurrently measuring gas permeability. Evolution of strain, porosity and permeability under mean stresses of 3.5, 7 and 14 MPa was measured. Permeability is measured by pulse transmission testing using N_2 and He as the saturant and assuming the validity of Darcy's law. Porosity is measured by pressure pulse with He as saturant and assuming an ideal gas. Experiments are conducted on a range of coals and biomass blends at mixtures of 100 percent coal through 100 percent biomass. Measured permeabilities are in the range 10^{-13} to 10^{-16} m^2 with the 100 percent biomass blends showing lower permeabilities than the coal biomass and 100 percent coal blends. Permeabilities change in loading and unloading and exhibit hysteresis. The data was fit to connect permeability with porosity using relations for porous media where permeability changes proportionally to the cube of the change in porosity. This model performs adequately since there is little size reduction in the granular mass due to the applied isotropic loading.

TABLE OF CONTENTS

LIST OF FIGURES

LIST OF TABLES

ACKNOWLEDGEMENTS

I owe my deepest gratitude to my mentor Dr. Derek Elsworth. It was pleasure working with him. He provided me the best opportunities at Penn state. I appreciate his patience, motivation, enthusiasm and immense knowledge which made my MS experience productive and exciting. He always encouraged me to think creatively. Thank you for being such wonderful person.

Special thanks to Dr. Chris Marone, Dr. Demian Saffer, Dr. Zuleima Karpyn and Ken Sprouse, Dr. Dirk VanEssendelft for their support, guidance and helpful suggestions.

I gratefully acknowledge the financial support provided by Pratt & Whitney, CA and National Energy Technology Laboratory, Morgantown, WV. Research was conducted at the Materials Research Institute, G3 Center for Geomechanics, Geofluids & Geohazards laboratory and Petrography Laboratory in the Geosciences Department all at Pennsylvania State University and was possible due with the help of the personnel at the locations.

I thank Shugang Wang, Divya Chandra, Hiroko Kitajima, Tom McGuire, Brett Carpenter, Marco Scuderi, Baisheng Zheng, Bryan Kaproth, Ghazal Izadi, Hemant Kumar, Jennifer Alpern, Julie Anderson, Katelyn Olcott, Matt Ikari, Matt Fry, Dan King, Julie Anderson, Alicia Cruz-Uribe, Taha Hussian, Takuya Isibashi and last but not the least Steve Swavely for their help and support.

Thanks also to my family. I am grateful for God’s provision of joys, challenges and grace for growth.

Chapter 1

Introduction

Background

Global development has put a significant demand on the need for affordable clean energy. Energy consumption in both the developed and the developing world is increasing with accelerating growth for developing countries. Electricity is produced primarily from non-renewable sources such as fossil fuels and nuclear power but also from renewable sources that include hydropower, wind, geothermal, solar and biomass. The United States is among one the largest consumers of electricity. The proportions of the different sources of power generation is shown in Figure1-1 with more than 65% of the power generated comes from fossil fuels (Electric Power Annual with Data for 2009, November 23, 2010). Coal remains a significant part of the energy portfolio in the U.S. as is also the case in the rest of the world. The United States has major proven coal reserves to satisfy increased energy demand along with renewables and nuclear (Libbin & Boehlje, February, 1977). These reserves are of high quality with most of the coal mined used for power generation (Moore, 1922).

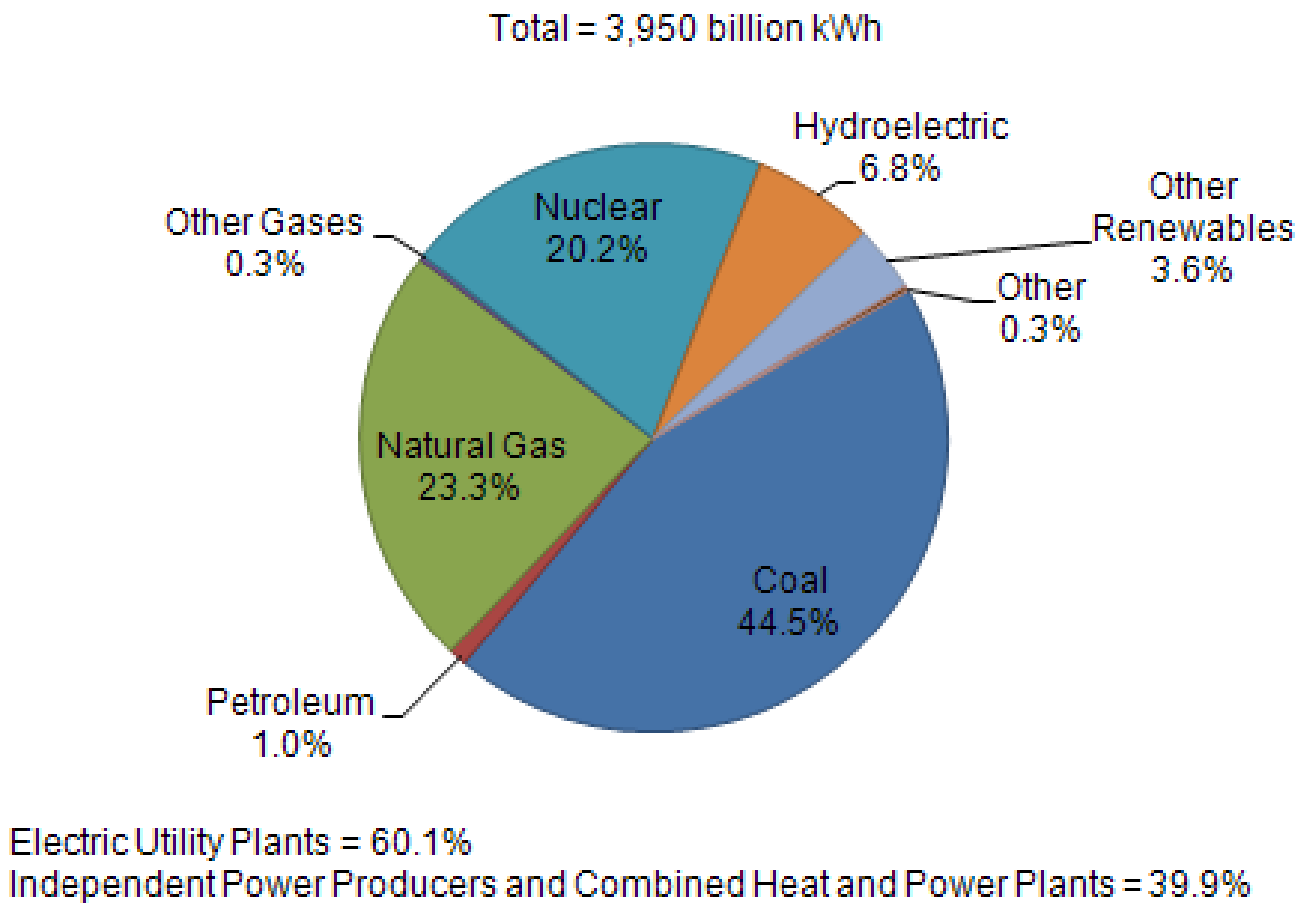

Figure 1-1 US electric power industry net generation (Electric Power Annual with Data for 2009, November 23, 2010)

Gasification

Carbon dioxide released into the atmosphere from anthropogenic source, including from power generation from coal, is suspected to contribute to global climate change.

The use of renewable sources of alternative energy, coupled with cleaner technologies which emit lesser quantities of carbon dioxide, can offset this challenge. Gasification is one such technology that can significantly reduce and even mitigate greenhouse gas emissions if oxygen from the air is separated and carbon dioxide is captured and possibly sequestered (Tavoulareas & Charpentier, July 1995). Simple coal gasification can be described with the three reactions (Schilling, Bonn, & Krass, 1981).

(a) Gasification with oxygen or air (partial combustion)

$$C + \tfrac{1}{2} O_2 \rightarrow CO$$

(b) Combustion with oxygen

$$C + O_2 \rightarrow CO_2$$

(c) Gasification with carbon dioxide

$$C + CO_2 \rightarrow 2CO$$

The basic water gas shift reaction that occurs after gasification converts carbon monoxide and water (as steam) to carbon dioxide and hydrogen with the hydrogen ultimately used as fuel (Ovesen, et al., 1996).

$$CO + H_2O \leftrightarrow CO_2 + H_2$$

In this arrangement, coal is fed into the gasifier where it is converted into synthesis gas, per the reactions identified above. Synthesis gas primarily consists of hydrogen, carbon monoxide, water, carbon dioxide and in small quantities methane, hydrogen sulphide, nitrogen, oxygen and argon (Cormos, Starr, Tzimas, & Peteves, June 15 2007).

Synthesis gas has a lower energy density compared to natural gas but this can be enhanced by removing particulates, sulfur, carbon dioxide, carbon monoxide and other gases. By this it is possible to recover high purity hydrogen. This may be combusted in a gas turbine in a typical integrated gasification combined cycle system where the byproduct of combustion is water, alone (Descamps, Bouallou, & Kanniche, December 12 2006) (Pronske, Trowsdale, Macadam, Viteri, Bevc, & Horazak, May 8-11 2006). Typically, in this process there are three groups of commercial gasification reactors: moving-bed, entrained-flow and fluidized-bed with entrained flow. Of these moving bed reactors are the most common in industrial applications (Zheng & Furinsky, May 3 2004) (Maurstad, September 2005). Coal can be fed into these types of gasifiers as a dry solid or coal-water slurry. The advantage of slurry feed system is it has lower capital cost over using a dry solid feed system but results in less efficiency known as cold gas efficiency. (Minchener, 2005)

It is also possible to either partly or fully replace coal with biomass. This offers a near-term alternative to fossil fuels (Hohenstein & Wright, 1994). Cofiring coal and biomass is a near term, low-cost option for reducing the carbon dioxide emitted into the atmosphere, biomass being carbon neutral (Sondreal, et al., 2001). There are still several technical challenges which need to be addressed before this technology can be implemented on a wider scale but with modifications the same gasification reactors used for coal gasification can accommodate biomass feeds (Beenackers, 1999). The environmental positives of power generation using biomass are carbon dioxide neutrality, low sulfur dioxide emissions and lower nitrogen oxide (NO_x) emissions when compared

with conventional coal fired power plants (Bain, 1993). Pressurized gasification with a gas turbine in a combined cycle mode, atmospheric gasification with a turbine or an engine and combustion with a Rankine cycle are the different ways of producing electricity by the thermal conversion of biomass (Bridgewater, July 26 1994). Advanced gasification technology allows for the utilization of compact long-lived and efficient gasifiers which increase performance and reduce capital costs over conventional methods (Fusselman, Sprouse, Darby, Tennant, & Stiegel, 2009). A significant amount of research has been conducted on gasification with respect to the fuels used, their mixtures, particle diameters, ambient temperatures of combustion, composition and flow velocity. Important characteristics for pressure feed into gasifiers require knowledge of both strength and permeability of the feedstock material to prevent blowback into the feed system (Dasappa, Paul, Mukunda, Rajan, Sridhar, & Sridhar, October 10 2004) (Sprouse & Matthews, June 17 2008).

Dense phase feeding

A critical component of the advanced gasifier is the feed system. A high pressure, ultra-dense phase, dry-coal feed system and multi-element injectors is a integral part in the development of advanced gasifiers which employ rocket engine technology (Sprouse, Widman, & Darby, Conceptual Design of an Ultra-Dense Phase Injector and Feed System, March 30 2006) (Sprouse, Widman, & Darby, Dry Coal Feed System and Multi-

Element Injector Test Plan, August 30 2006). The success of the multi-element which allows for better mixing of fuel and oxygen is dependent upon a feed system which can allow for feed entering of feed at different locations in the gasifier. This is possible with a system of pipes transporting feed to individual locations in the gasfier. A continuous high-pressure dense-phase feed system has been studied in detailed and by maintaining ideal pressure conditions inside the transport pipes it is possible to achieve flow without having plugs in the flow (Burge, Roberts, & Zettle, 1964) (Sandy, Daubert, & Jones, 1970) (Friedman J. , 1979) (Combs, Ubhayakar, Breese, Kahn, & Lee, 1980) (Oberg, Falk, Hood, & Gray, 1977) (Oberg, Falk, Kahn, & Combs, 1982). The various flow regimes of fluid-solid two-phase transport in a horizontal tube is shown Figure 1-2. A dense-phase – uniform plug flow allows for maximum transport of solids.

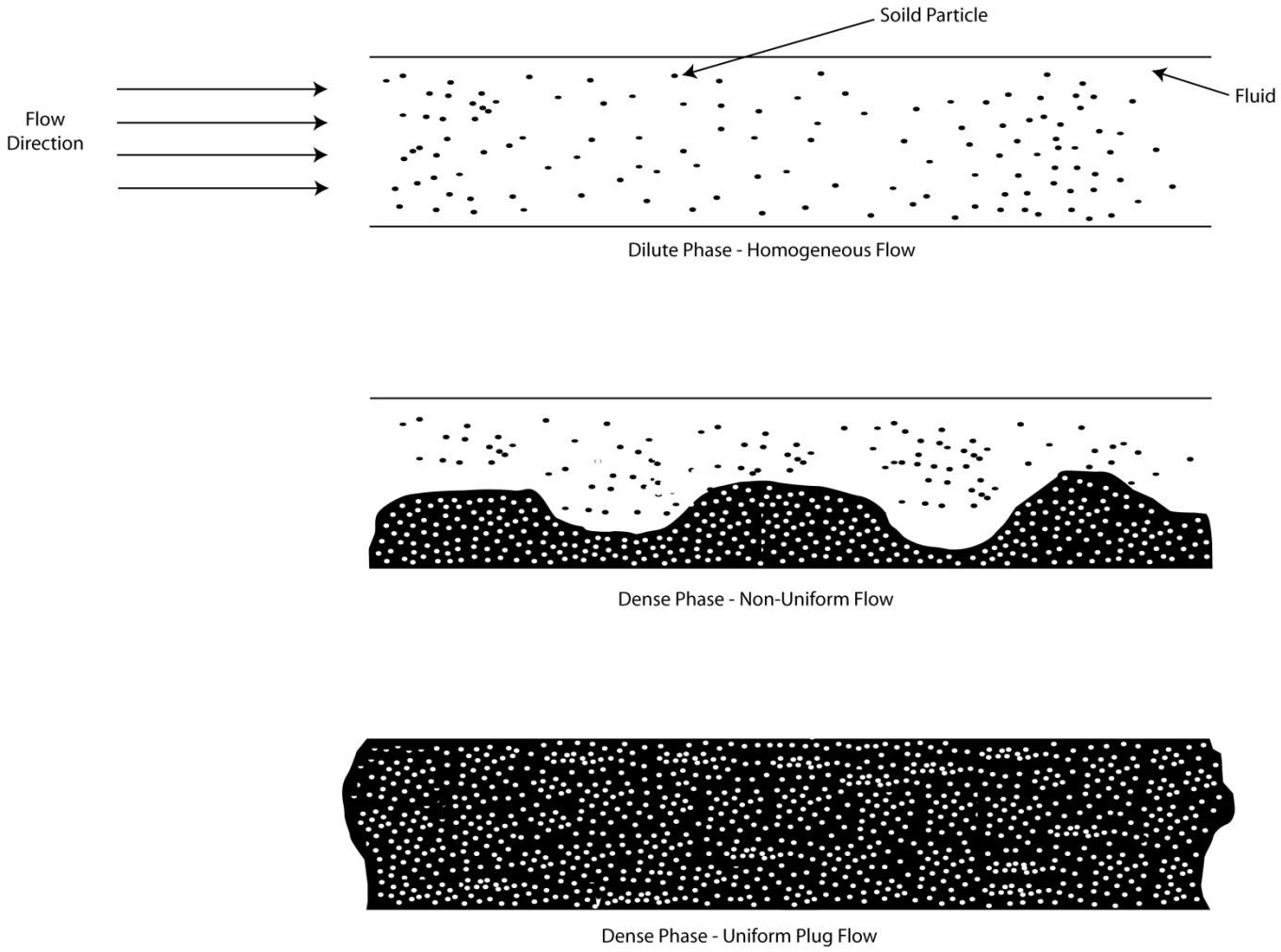

Figure 1-2 Flow regimes of fluid-solids two phase transport in a horizontal tube (Sprouse & Schuman, November 1983)

The transport of solids with the help of the gas depends upon a number of different parameters which have complex relationships with flow velocities such as gas and solid densities, gas viscosity, pipe and particle diameters and the gas-solids void fraction (Klinzing, 1981) (Wen & Obrien, 1976). The void fraction has a direct relation with the

porosity which controls permeability. Porosity is directly related with the applied stress on the feed. Stress is applied to the feed to make sure it is in ultra-dense phase as it reduces amount of gas needed for transport, reduces power requirement and also makes the system more compact (Sprouse & Schuman, November 1983). The feed system developed consists of two moving conveyer belts applying stress on the dry feed. Stress applied to the feed maintains pressure inside the gasifer. The main focus of the work presented in this thesis is to study the porosity and permeabilities of various feeds for the gasifiers. A verified relationship between permeability and porosities for coal and biomass feeds with nitrogen which is used to transport the feed would make it easy to change feed to the gasifier by only changing the applied stress and it would be possible to use the same system for a variety of feeds.

Permeability porosity relationships

This work looks to establish a relationship which links permeability and porosity for gasifier feeds. Prior studies on porous rock, sands, clays and soils define relations between porosity and permeability (Kozeny, 1927) (Carman, Flow of Gases through Porous Media, 1956) (Terzaghi, 1925) (Griffiths, 1958) (Kotyakhov, 1949). A typical model is based on the Kozeny-Carmen relationship. This is a simple capillary tube model that uses the concept of hydraulic radius (Bear, 1972). The Kozeny-Carmen relation is

the starting point for many other models and has been widely reported (Xu & Yu, 2008) (Costa, 2006). This relationship defines permeability as

$$k = \frac{1}{K_0 \cdot T^2 \cdot S_0^2} \cdot \frac{\gamma}{\mu} \cdot \frac{n^3}{(1-n)^2} \qquad (1)$$

where k is the permeability, K_0 is pore shape factor, T is turtuosity of the flow path, γ is density of the permeating fluid, μ is viscosity of permeating fluid, S_0 is specific surface of the grains and n is the porosity. Specific surface of grains is measured with particle size assuming spherical particles per unit mass while porosity is bulk connected porosity of sample.

Based on this relation, a variety of other correlations have been developed to fit specific porous media (Taylor, 1948) (Samarasinghe, Huang, & Drnevich, 1982) (Olson & Gholamreza, 1970) (Brown, 1991). Various in-situ studies have determined relationships between permeability and porosity (Ehrenberg & Nadeau, 2005) (Amthor, Mountjoy, & Machel, 1994) (Schutjens, et al., 2001). However, there are a few relations between permeability and porosity which are valid for all types of porous media and fluids. In sandstones, intrinsic permeability is a function of grain size, mean grain shape, sorting and grain packing. Grain size and grain packing in turn determine pore size while grain packing determines porosity (Berg, 1970) (Chilingar, 1963) (Friedman M. , 1976). The rate of reduction in porosity and permeability of mudstones during compaction depends strongly on lithology, described for example by grain size. As porosity decreases with compaction due to preferential collapse of the larger pores, the porosity-permeability trends converge (Dewhurst & Aplin, January 10 1998). The influence of grain size on

compressibility and permeability of mudstones is well documented (Aplin, Yang, & Hansen, April 25 1995) (Skempton, 1970) (Burland, 1990). The permeability of intact soft clays is a function of void ratio, grain size, plasticity and the fabric of the clay (Tavenas, Jean, Leblond, & Leroueil, September 22 1982). In rocks the permeability-porosity relationship and the relative reduction rates on application of stress are primarily dependent on pore geometry and connectivity, fluid–mineral interfacial energies, temperature and chemical reactions (Bernabe, Brace, & Evans, 1982) (Holness & Graham, 1991) (Brantley, 1992) (Olgaard & Fitz Gerald, 1993) (Somerton & Mathur, 1976). The first original work on permeability and porosity relationships was based on the simple capillary tube model (Blake, 1922) (Kozeny, 1927). After verification, various models with modifications have been proposed (Carman, Permeability of Saturated Sands, Soils and Clays, 1939) (Carman, Fluid Flow through Granular Beds, 1937) (Chapuis & Aubertin, 2003). Empirical relations have been developed using the Kozeny-Carman equation relating to various porous media with similar power exponents to the one used in the model in this paper (Timur, 1968) (Chapius, 2004) (Zhang, Paterson, & Cox, August 10 1994).Based on experimental data collected, empirical equations are popularly used in the oil and gas industry to calculate permeability (Nelson, 1994).

It is desired to fit a simple relationship between porosity, permeability and the grain-size distribution of the porous medium (Chillingar, 1964).

$$k = \frac{d_e^2 \cdot \phi^3}{72 \cdot (1-\phi)^2} \quad (2)$$

where k is the permeability, ∅ is porosity and d_e is the effective diameter of the individual grains again assuming spherical particles. Keeping grain diameter constant and changing only the porosity enables changes in permeability to be defined in terms of cubic dependence (Liu, Chen, Elsworth, Qu, & Chen, 2011).

$$\frac{k}{k_0} = \left(\frac{\phi}{\phi_0} \right)^3 \quad (3)$$

A similar power law dependence of the permeability to the total porosity has been fitted within a certain range to other porous media as well (Zhang, Paterson, & Cox, August 10 1994) (Chapius, 2004). Under these constraints the model is fit to the data recovered in this study.

Chapter 2

Experimental Techniques

Permeability is measured by end-to-end pulse testing from upstream to downstream reservoirs using the standard triaxial apparatus of Figure 2-1. The pressure-pulse time-decay method is used. Dry cylindrical samples (2" long and 1" diameter) of powdered coals are sheathed in shrink-wrap and held between two ends of the triaxial core holder (Temco). Detailed photo documentation of the process is in Appendix A. Confining and axial pressures are applied by using two syringe pumps (ISCO 65D) with the capability of applying 14500 psi (100 MPa) and with a volume of approximately 68 ml. The pumps use water to apply stress to the sample. Axial stress is applied at one end by pushing a piston by hydraulic pressure while confining pressure is applied by a confining fluid around the sheathed sample. The upstream reservoir has an approximate volume of 30.5 ml while the volume of the downstream reservoir is approximately 17.9 ml. Valves along the tubing connect the core to the reservoirs and regulate flow of gas to the sample. Two end platens at either end of the sample allow for flow to and from the upstream and downstream reservoirs respectively. Pressure of the permeating fluid in the upstream and downstream reservoirs is measured by two separate pressure transducers (Omega PX302-2KGV) which have a range of 2000 psi (14 MPa) and to a resolution of less than 10 psi (0.06 MPa). Pressure is controlled and recorded using a data acquisition card and via

Labview with sampling at 10 Hz. Based on the data recorded by the two individual drivers a single data file is created with the pressure data from the transducers and also the applied stresses from the pumps.

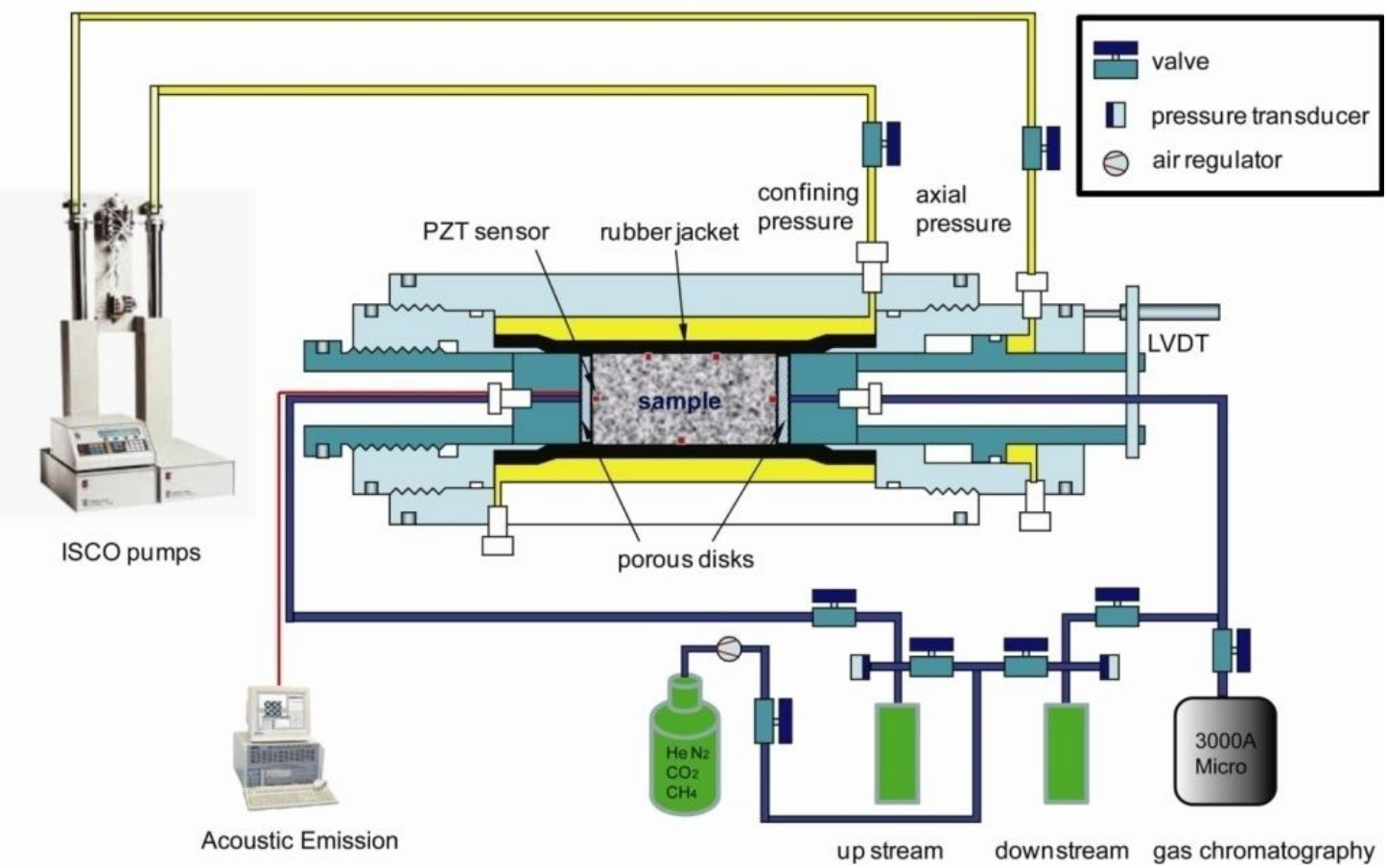

Figure 2-1 Permeability testing tri-axial setup (Wang, Elsworth, & Liu, July 2011)

Sample preparation

The sample material is prepared by grinding coal and biomass to a granular powder of between 20 and 200 mesh. The sample is built by first placing shrink-wrap tubing over the first platen end with the empty tubing pointing upwards. We insert a frit on the platen face and then fill this open tube with sample to a height of two inches. A frit and second platen is then inserted on top of the sample. An additional wrap is placed around the sample to ensure no leakage. Spacers are placed at either end of the platen assembly to make the desired length for the triaxial vessel holder. Everything not covered by the shrink-wrap is covered by rubber jackets. All of these are tied with metal wires to prevent the confining fluid from leaking into the sample or out of the vessel. The sample is then loaded into the vessel and the open end is closed but with the flow lines exiting the pressure vessel. These lines are then connected to the upstream and downstream reservoirs. The detailed sample preparation procedure is included in Appendix A.

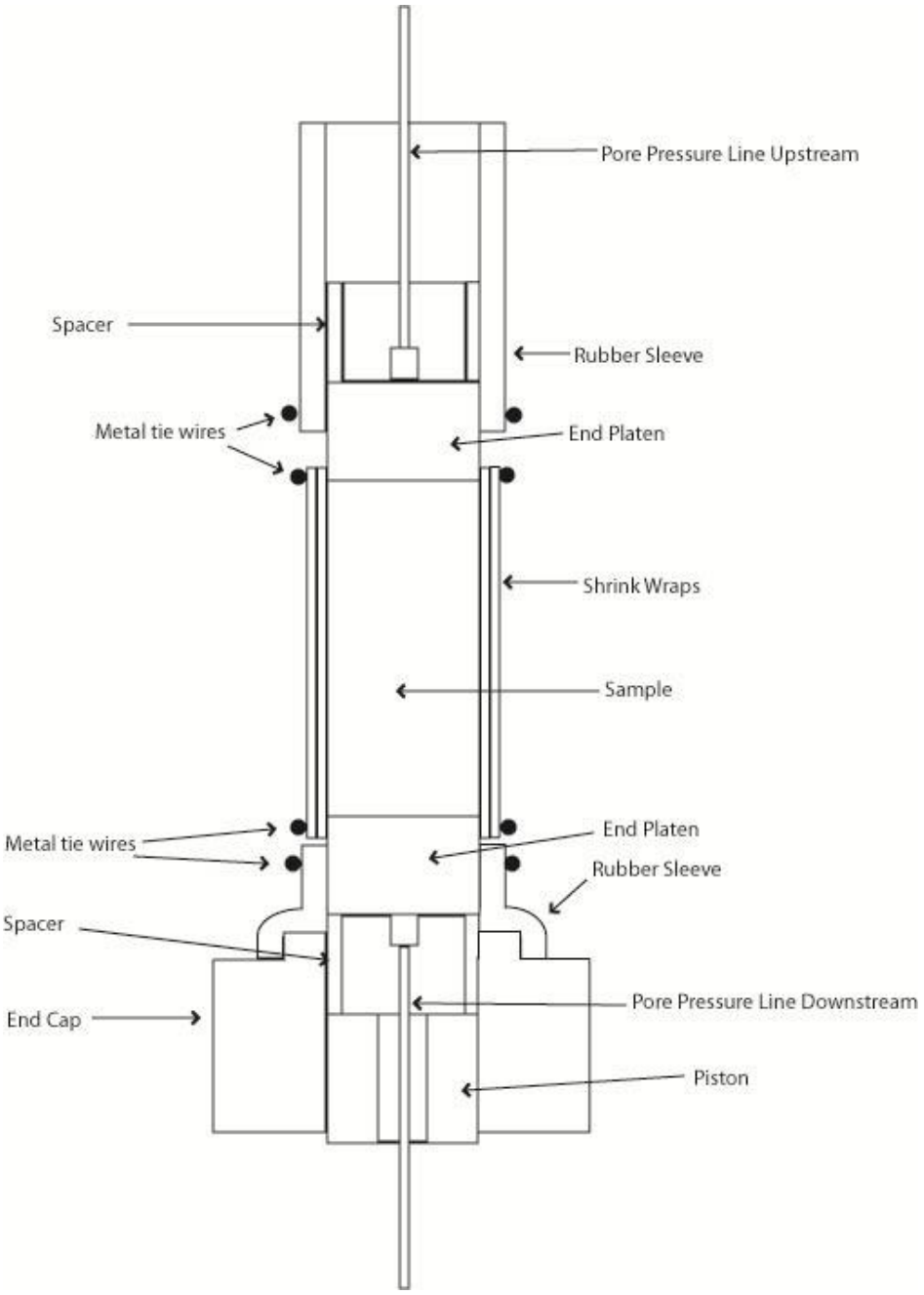

Figure 2-2 Schematic of typical sample assembly

Permeability and porosity measurements

Permeability is measured by pulse testing for low permeability samples. This method records the decay of pressure assuming the validity of Darcy's Law (Brace, Walsh, & Frangos, March 15 1968) (Hsieh, Tracy, Neuzil, Bredehoeft, & Silliman, 1981). These permeability methods are mainly used to measure the response of low permeability porous media where the time taken to achieve equilibrium is high (Neuzil, Cooley, Silliman, Bredehoeft, & Hsieh, 1981). In this case the measurements are in moderate permeability samples but with significant equilibration times and this method remains valid (Jones, March 1997) (Zeynaly-Andabily & Rahman, 1995). The results obtained by pulse decay technique are comparable with those achieved by steady state flow using Darcy's Law. Permeability is calculated based on the relation,

$$k = \frac{\alpha \cdot \mu \cdot \beta \cdot L \cdot V_{up} \cdot V_{dn}}{A \cdot (V_{up} + V_{dn})} = \frac{\alpha \cdot \mu \cdot L \cdot V_{up} \cdot V_{dn}}{A \cdot P_{eq} \cdot (V_{up} + V_{dn})} \qquad (4)$$

where k is the permeability of the sample, A is the cross-sectional area of the sample, L is the length of the sample, μ is the dynamic viscosity of the gas, β is the compressibility of the gas (assumed to be $1/P_{eq}$), and P_{eq} is the system equilibrium pressure (equal to P_f if upstream pressure and downstream pressure converge at the end of the test). P_{up} is the upstream reservoir pressure, P_{up}^0 is the initial upstream reservoir pressure, P_f is the final equilibrium pressure in the system, P_{dn}^0 is the initial downstream reservoir pressure, $V_{up}$is the upstream reservoir volume and V_{dn} is the downstream reservoir volume. The

magnitude of α is calculated by plotting a log-based decay curve of pressure vs time as shown in Figure 2-3 where the relation between pressure and reservoir volumes and time is given as

$$\left(\frac{P_{up}-P_{eq}}{P_{up}^{0}-P_{dn}^{0}}\right)\cdot\left(\frac{V_{up}+V_{dn}}{V_{dn}}\right)=e^{-\alpha\cdot t} \qquad (5)$$

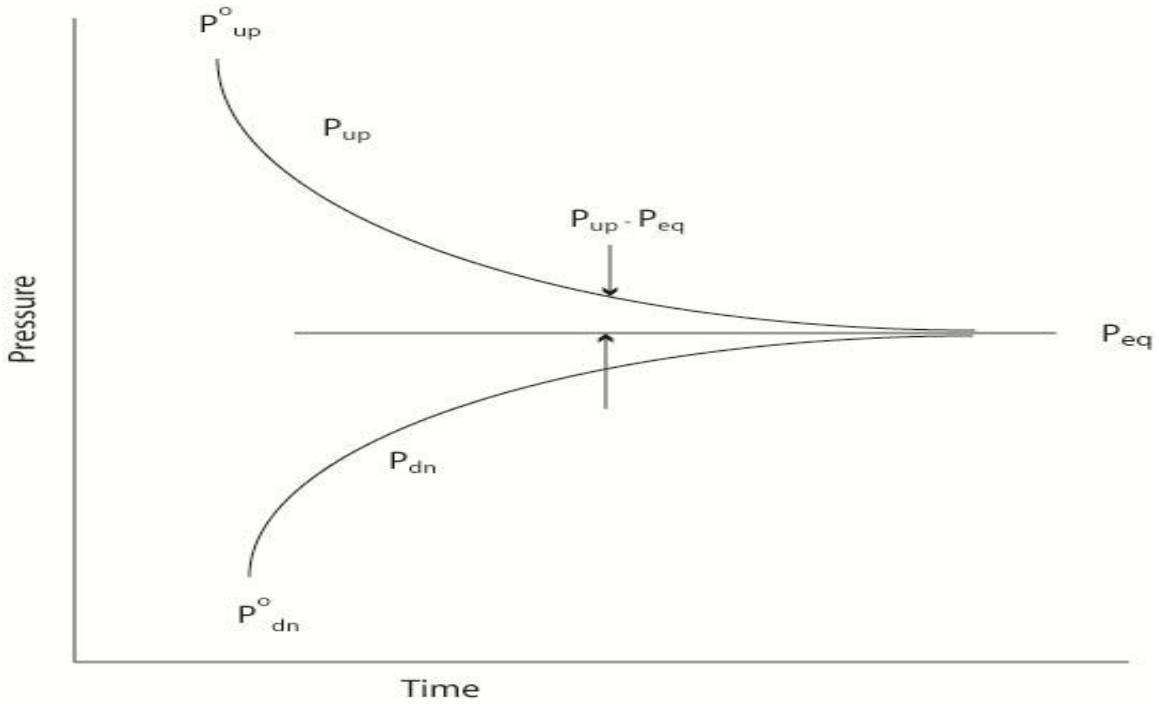

Figure 2-3 Typical pressure decay plot of upstream and downstream pressure vs time

Porosity of the sample aggregate is recovered from the absolute magnitude of the pressure change available from the same data. This is completed for the sample saturated with Helium – an inert gas that will not sorb onto the sample substrate. This measures connected porosity and was checked by measuring with both Helium and Nitrogen – both near ideal gases at the pressures in used (Rodrigues & Lemos de Sousa, 2002).

Chapter 3

Experimental Observations

A series of 33 experiments were run on 11 different samples to determine porosity and permeability at different confining stresses. For each sample permeability was measured at confining stresses of 500 psi, 1000 psi and 2000 psi using nitrogen as the permeating fluid. These permeability measurements were calibrated against porosity measurements measured keeping pressure in the upstream reservoir at 60 psi (0.4 MPa) and pressure of downstream reservoir at atmospheric pressure, 14.7 psi (0.1 MPa). The apparatus had upstream and downstream reservoir characteristics as identified in Table 3.1. The sequence of experiments and in particular the coal to biomass blends are as identified in Table 3.2.

Table 3-1 Experimental constants

Experimental constants	Value	Units
Volume upstream	30.58	ml
Volume downstream	17.94	ml
Viscosity of fluid	0.0000174	Pa.s
Area of cross section of sample	506.77	square millimeters
Length of sample	50.8	millimeters

Table 3-2 Experimental matrix

Material Details Coal %	No Biomass Material	Corn Stover Pellets +200 Mesh Barrel	Corn Stover +200 Mesh Barrel
No Coal Material 100% Biomass		0	0
Powder River Basin (PRB) Subbituminous	100	75	
Illinois # 6 Bituminous	100		90
North Dakota Lignite	100		75
Powder River Basin (PRB) Transport Subbituminous	100		
Powder River Basin (PRB) Subbituminous High Moisture Content	100		
Mississippi Lignite	100		

Permeability data

The porosity and permeability of a total of 11 coal and biomass mixtures were measured at hydrostatic conditions. The stresses applied to the sample were 500 psi (3.5 MPa), 1000 psi (7 MPa) and 2000 (14 MPa) psi respectively. Permeabiltiy of the samples with nitrogen as the permating fluid was measured as defined previously by recording the equilibration of pressures with time. The change in pressure with time is plotted for both upstream and downstream reservoirs. In ideal conditions the two should meet at equilibrium pressure. The equilibrium pressure is then substacted from the pressure in the upstream reservoir and then plotted vs time on a semilog plot. The slope of the resulting line gives the value of α which is used to calculate permeability using equation 4. As an overall trend, measurements of permeabiltiy show a decrease in permeability with a decrease in porosity. Biomass blends have the highest permeabilities while coal and coal-biomass blends display the lowest permeability.

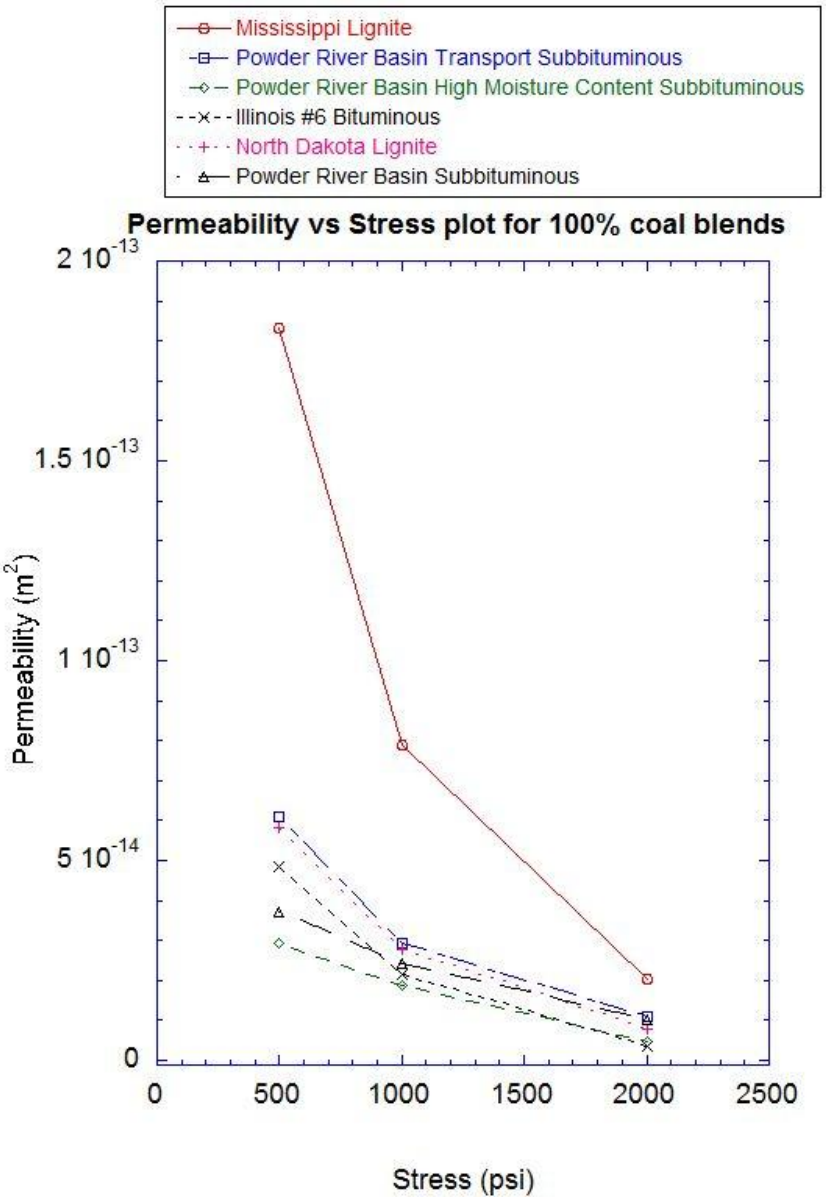

Figure 3-1 Permeability vs stress plot for coal blends

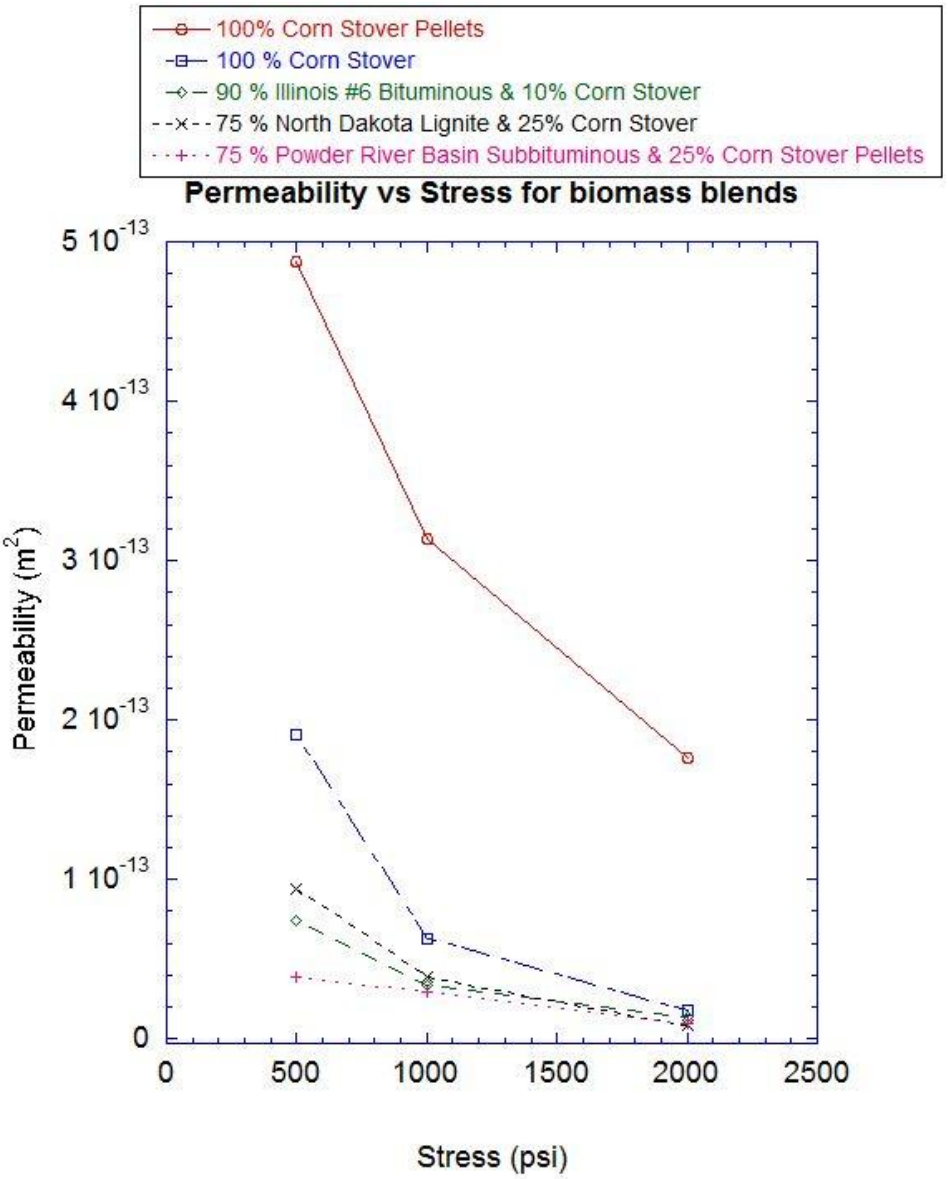

Figure 3-2 Permeability vs stress plot for biomass blends

Porosity data

Porosity is also measured with the applied hydrostatic stress as shown in figure 3.3 and 3.4. Porosity decreases with an increase in stress as the sample compacts and the void space decreases. The reduction in porosities does not follow any universal trend and maybe dependent on factors not included in this study. The porosity decreases rapidly after the initial application of stress and then decreases more slowly as stress is subsequently increased. This is also evident with the decrease of permeability being greater at the beginning of application of stress and decreasing as stress is increased. Permeability is not dependent on porosity alone but is also a function of the individual material. The decrease in permeability with increase in applied stress does not show any trend for the different samples. Both porosity and permeability have complex relations with applied stress.

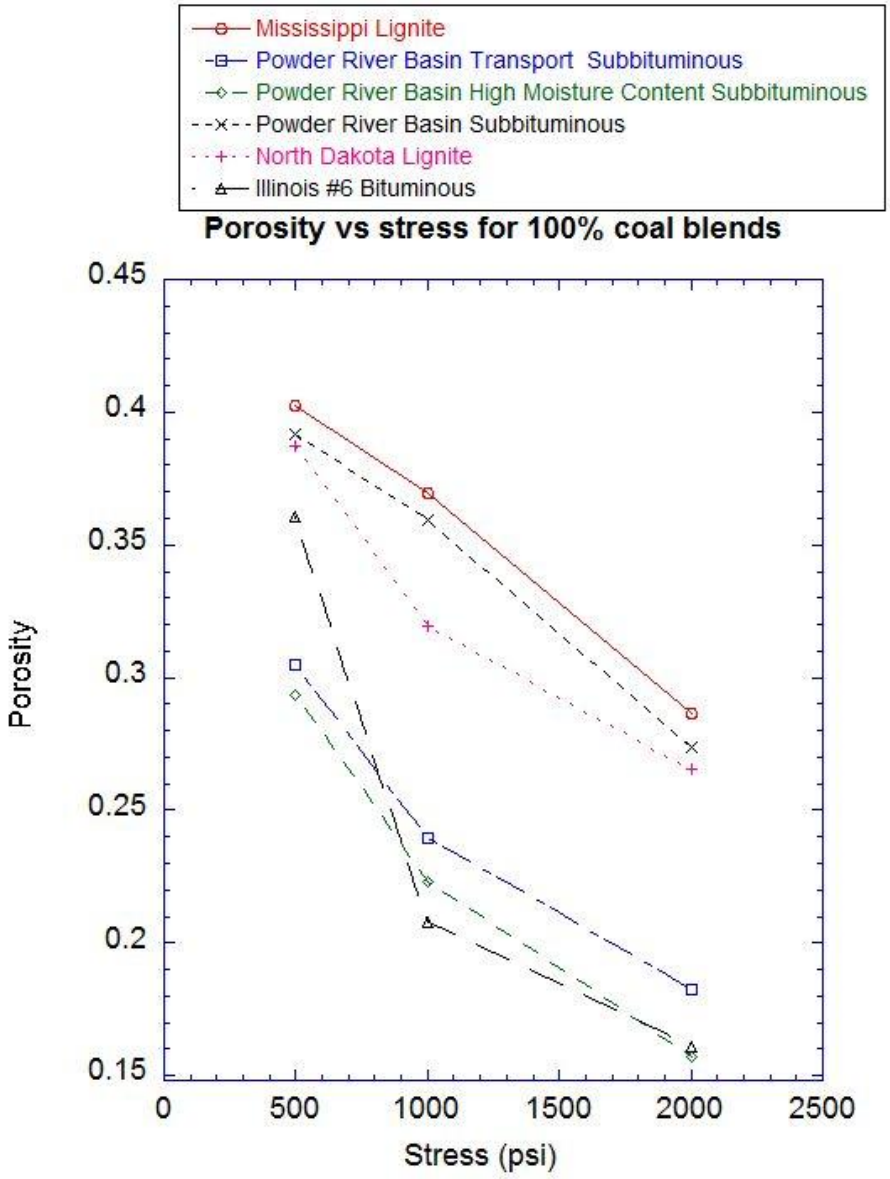

Figure 3-3 Porosity vs stress plot for coal blends

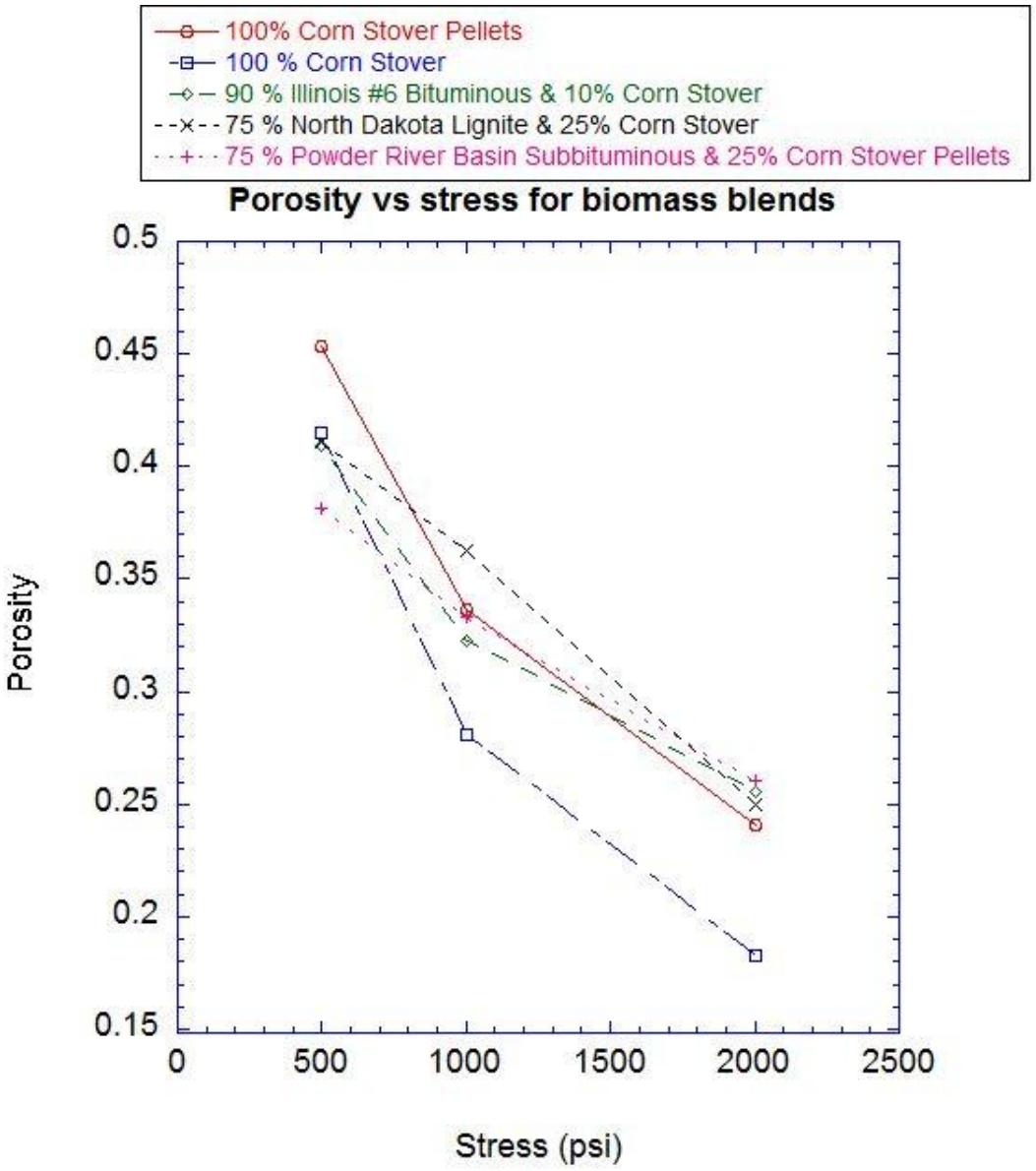

Figure 3-4 Porosity vs stress plot for biomass blends

Particle size analysis

Particle size analysis has been performed using a Malvern Mastersizer capable of measuring particle sizes from 0.0582 microns to 900 microns. Ethanol was used as the solvent to disperse the coal particles properly. Once sized and doped with solvent, the sample was not used for a permeability experiment. Thus the pre-test grain size measurements are for surrogate samples rather than those for which permeability was later directly measured. However, post-test grain size measurements were for the permeability-measured samples. The post-test samples were taken from the centre and end of the sample. The pretest samples in Figure 3-5 shows that there is considerable difference in particle sizes and should not be misinterpreted as reduction in grain size during the application of stress. There is no apparent reduction in the size of the particles post-test. Thus a permeability model that accounts only for changes in permeability due to changes in porosity, and not grains size, may be used in the following.

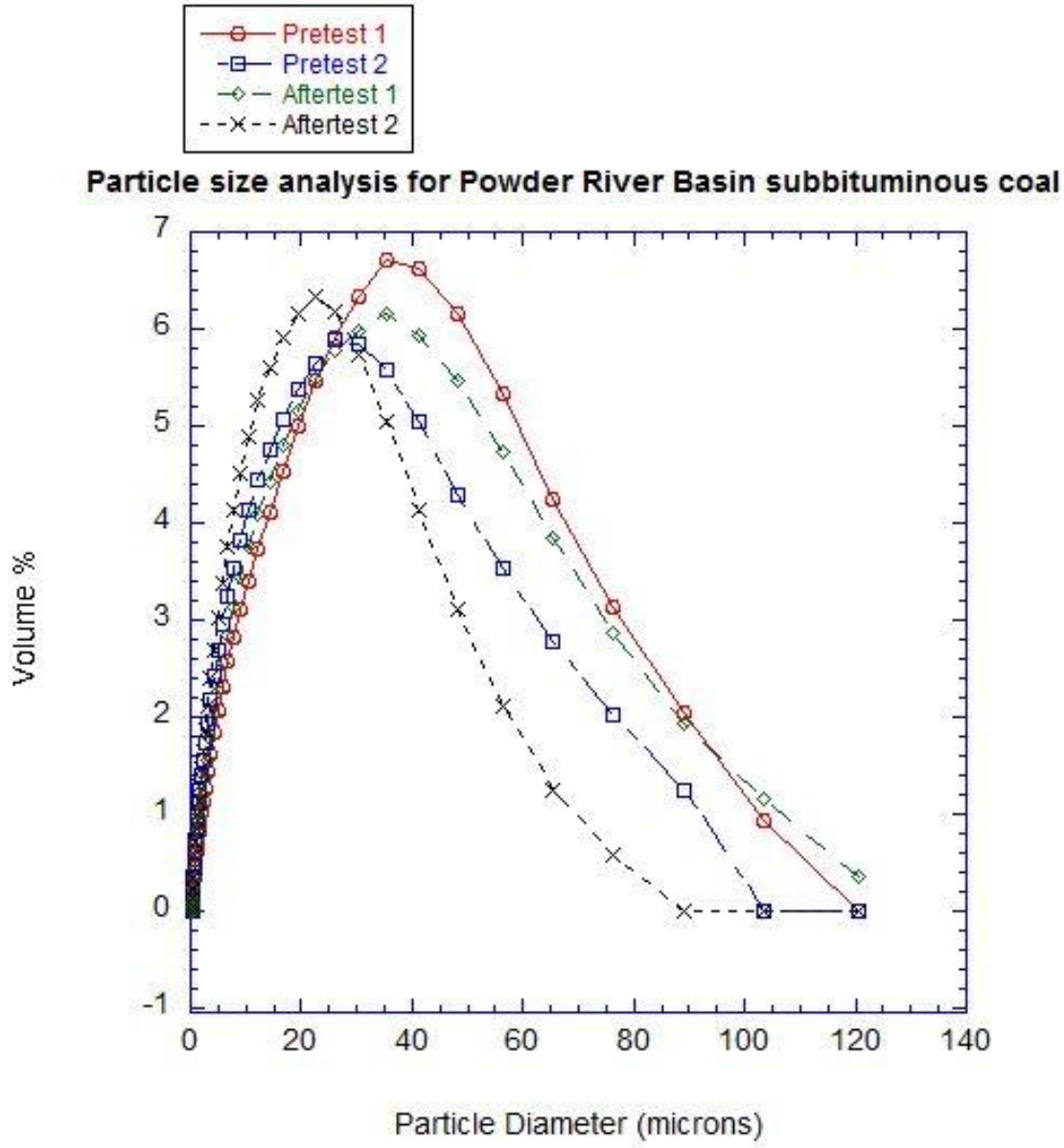

Figure 3-5 Particle size analysis for Powder River Basin subbituminous coal

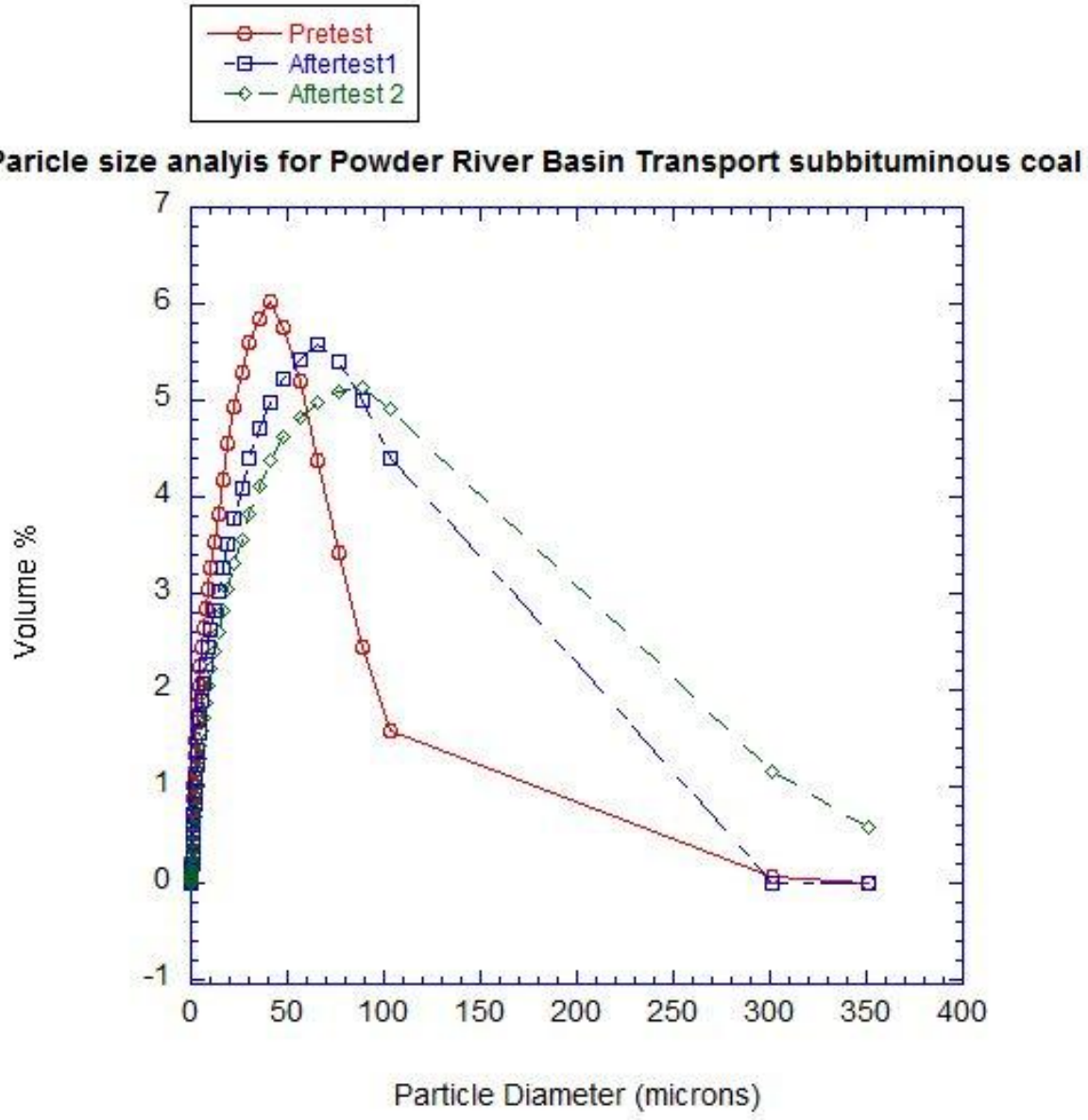

Figure 3-6 Particle size analysis for Powder River Basin Transport subbituminous coal

Chapter 4

Model

The tube models are the one of the simplest models from which Darcy's law may be derived. Flow through porous media is governed by Darcy's law. The capillary tube model is illustrated in figure 4.1 below.

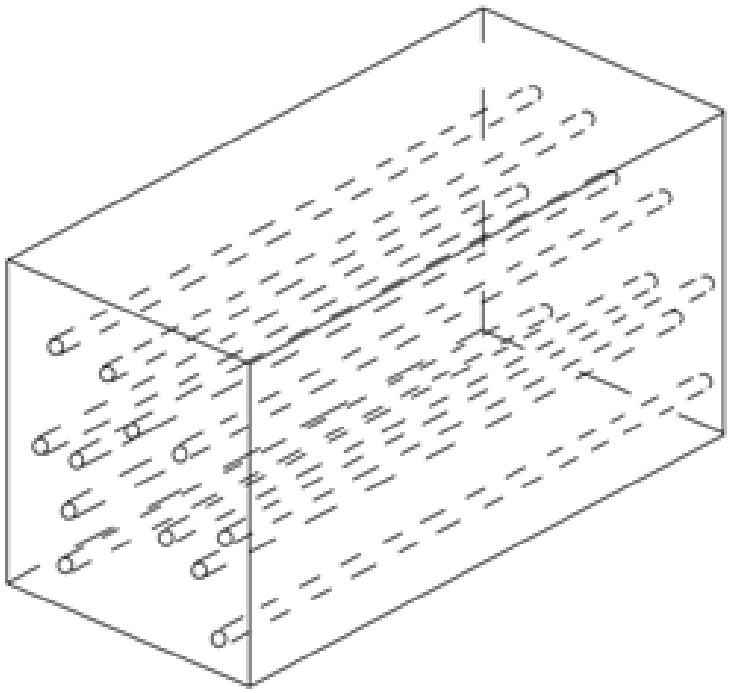

Figure 4-1 Capillary tube model (Bear, 1972)

The capillaries are shown as parallel tubes with the same diameter but can be of different diameter and can also exhibit tortuosity. The relationship $k/k_0 = (n/n_0)^3$ is based on this. This model assumes that the diameter of the tubes have a relationship to the pore size distribution. The model $k/k_0 = (n/n_0)^3$ is a good fit for the data but with limited data points. Applying the sample to hydrostatic stress is an unrealistic assumption in practical applications as $\sigma_1 \neq \sigma_3$ in reality. This is only for the purpose of the study where we assume ideal situation. Most of the blends show a linear trend. The bituminous and subbituminous coal blends in figure 4.2 show a better fit than the lignite blends. This is also seen in the 100% biomass and bituminous and subbituminous coal biomass blends displaying a better fit to the data as compared to the lignite coal biomass blends. If the data set is expanded it would be possible to find a closer fitting curve for the model. The next set of data points does exactly this. The subbituminous coal blends were chosen for extending the data because there were two types of the same coal type. Also both subbituminous coals are from the same Powder River Bain (PRB) region. It would be possible to generate better data for fitting the model with these samples is the presumption.

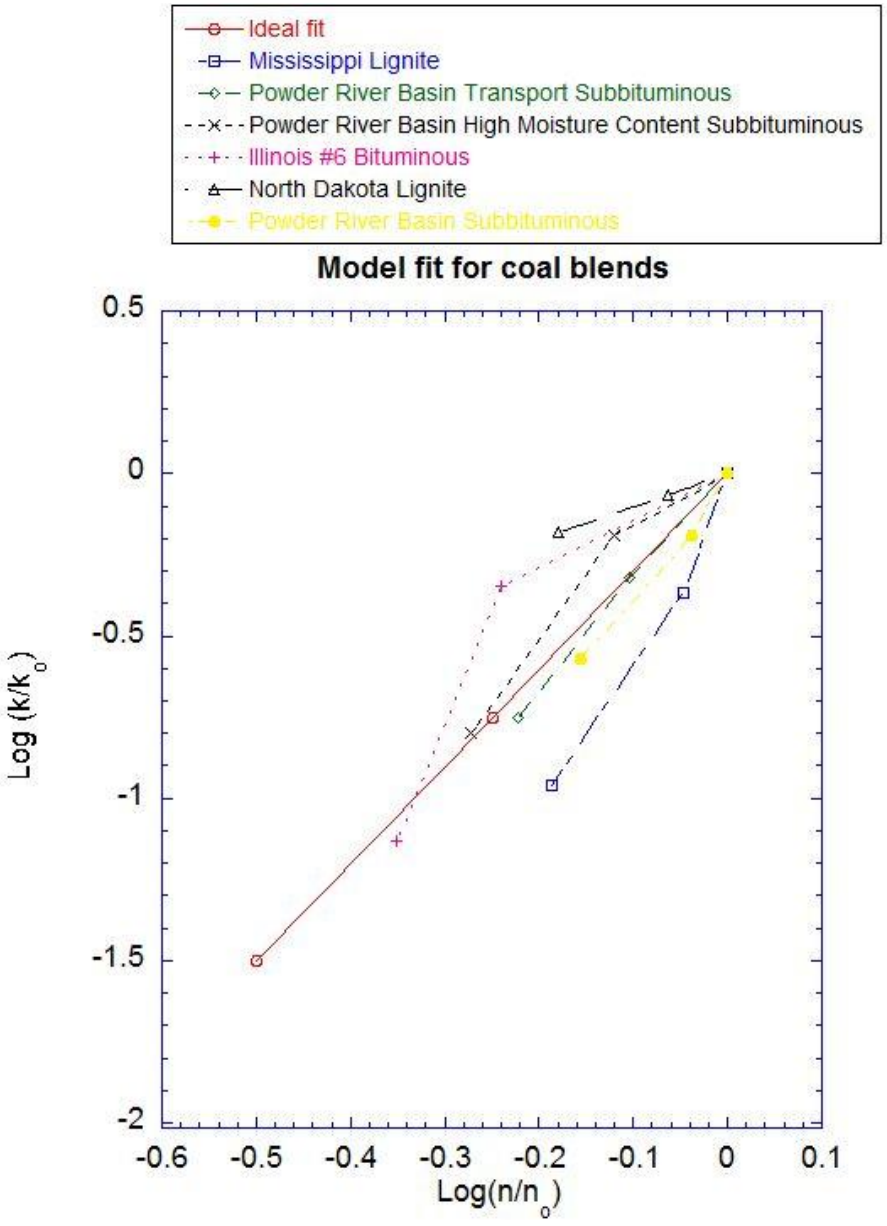

Figure 4-2 k/k_0 vs n/n_0 for coal blends

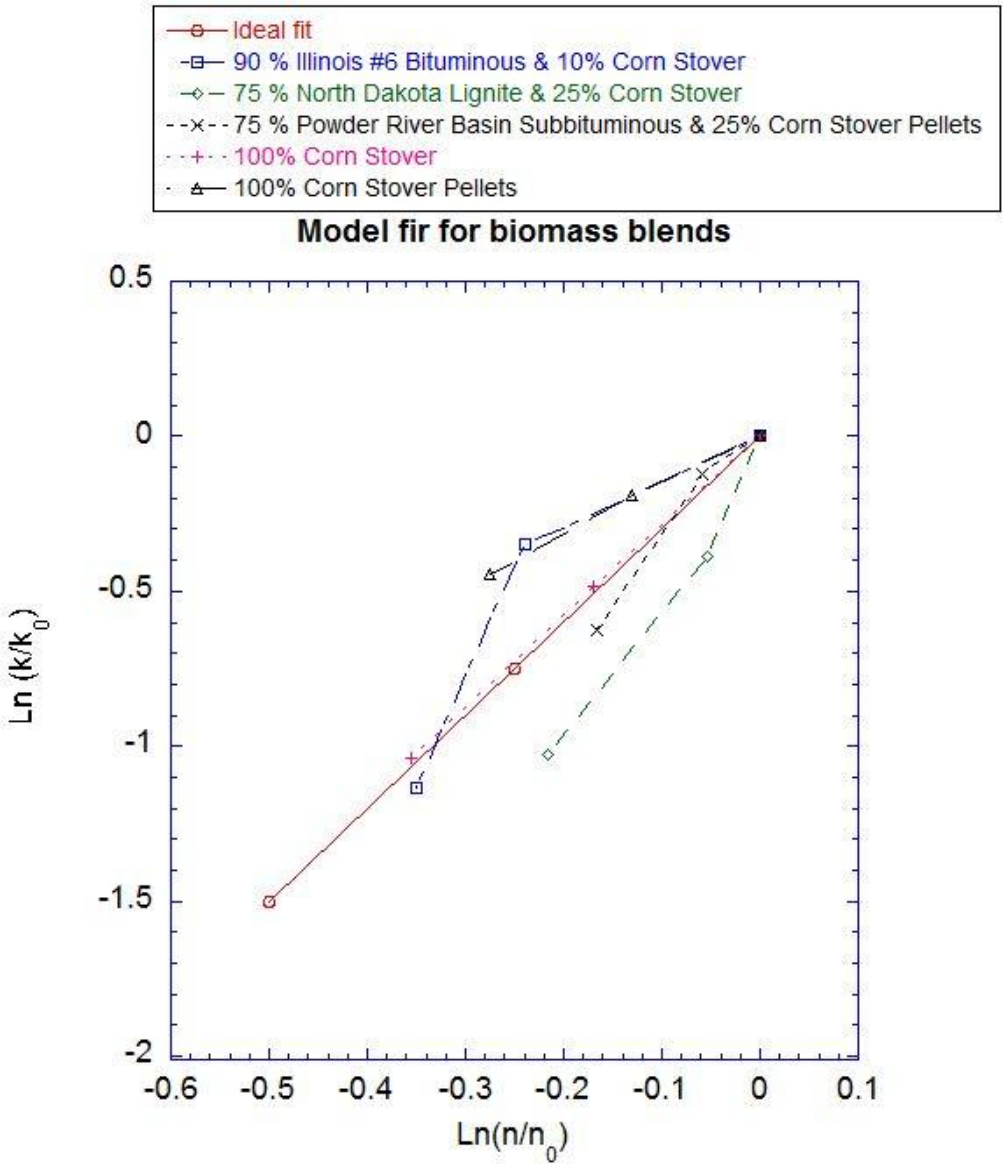

Figure 4-3 k/k_0 vs n/n_0 for biomass blends

Powder River Basin (PRB) subbituminous data

The data set is expanded in order to get a better fit for the model. Permeability and porosity was measured at 1 MPa (145 psi), 2 MPa (290 psi), 3 MPa (435 psi), 5 MPa (725 psi), 10 MPa (1450 psi) and 15 MPa (2175 psi). This doubles the initial data set. Using this data k/k_0 vs n/n_0 plot is created for the subbituminous coal blends. In this case, we get the exponent almost equal to 3 which fit the model proposed in this paper. The Powder River Basin subbituminous and Powder River Basin Transport subbituminous coals were selected to extend the data set as we had data on subbituminous coal samples and so it is possible to validate the achieved results.

Table 4-1 Powder River Basin subbituminous data

Stress	Permeability (m^2)	Porosity
1 MPa (145 psi)	8.37×10^{-14}	0.4413
2 MPa (290 psi)	6.21×10^{-14}	0.4348
3 MPa (435 psi)	4.99×10^{-14}	0.3795
5 MPa (725 psi)	3.58×10^{-14}	0.3221
10 MPa (1450 psi)	1.31×10^{-14}	0.2423
15 MPa(2175 psi)	7.83×10^{-15}	0.2233

Table 4-2 Powder River Basin Transport subbituminous data

Stress	Permeability (m^2)	Porosity
1 MPa (145 psi)	2.20×10^{-13}	0.4158
2 MPa (290 psi)	1.44×10^{-13}	0.3768
3 MPa (435 psi)	1.15×10^{-13}	0.3590
5 MPa (725 psi)	6.36×10^{-14}	0.3147
10 MPa (1450 psi)	2.62×10^{-14}	0.2294
15 MPa(2175 psi)	1.24×10^{-14}	0.1998

Strain data for the two tests were also recorded. Strain increases with application of stress. Figure 4.5 shows strain hardening. Strain rate was kept constant at ~10^{-6} /s. This path is common in other sedimentary rocks and is well studied (Wang & Park, 2002) (Shiping, Yushou, Yi, Zhenye, & Gang, 1994). Application of stress was not uniform and permeability was not measured continously which may explain the non-linear strain induced. Large strain is produced with application of low stress and strain induced reduces as stress increses.

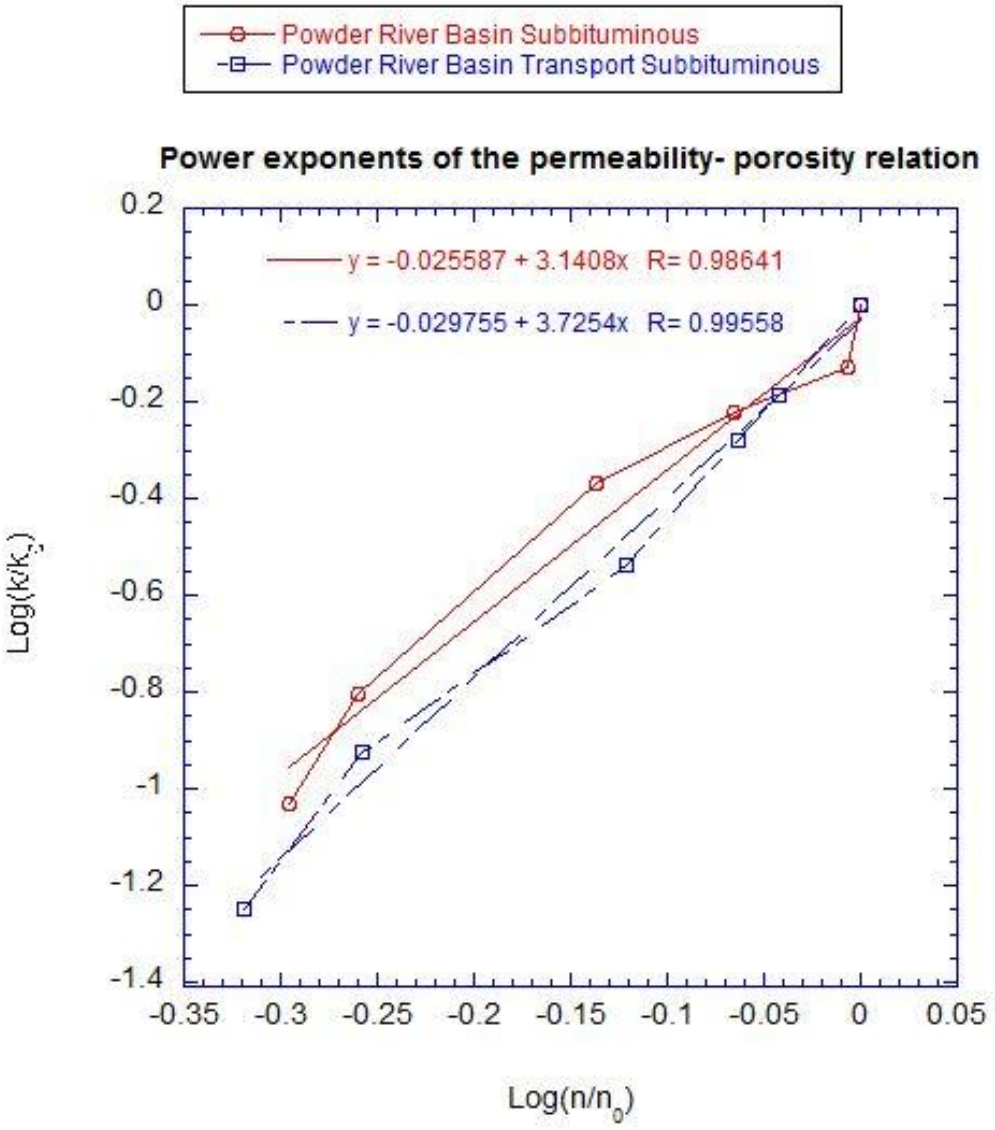

Figure 4-4 Exponents of slope for subbituminous coals

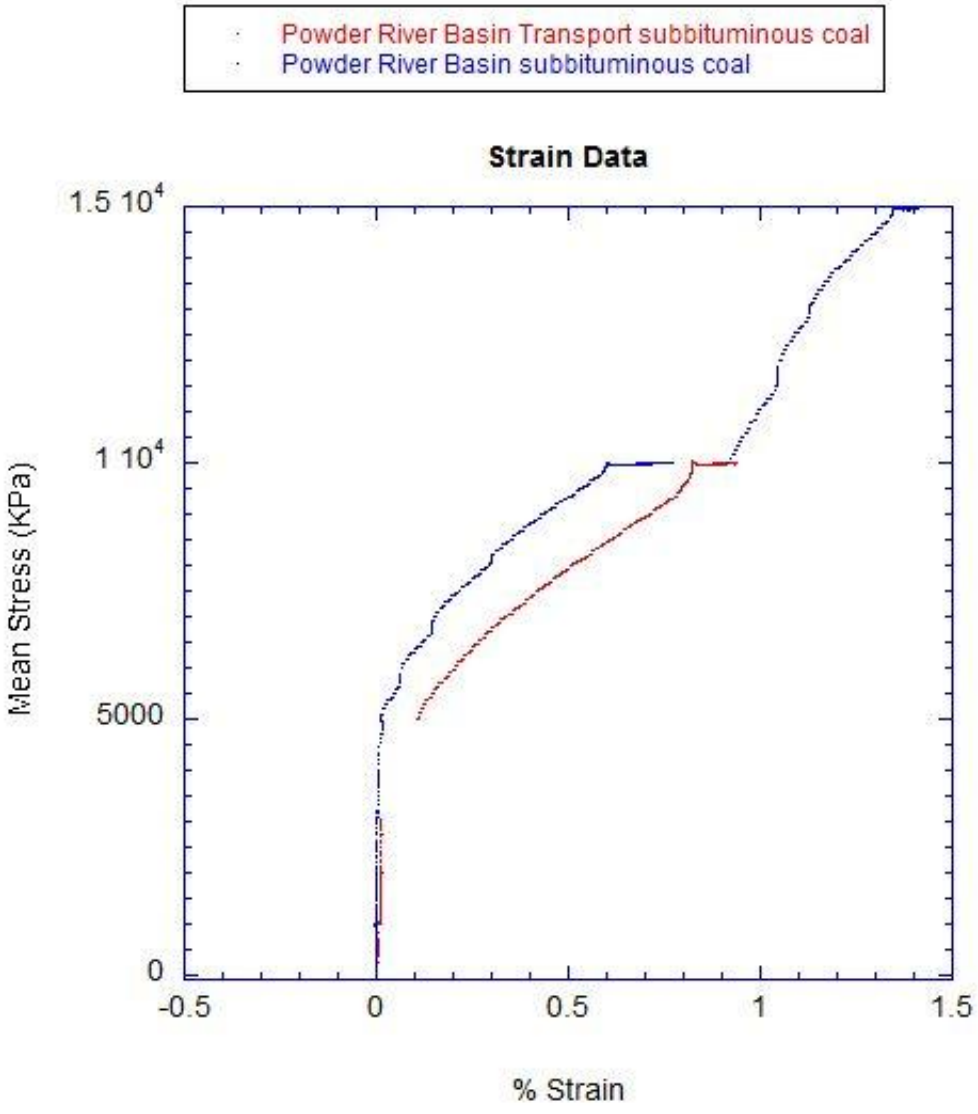

Figure 4-5 Axial strain vs mean stress for subbituminous coals

Chapter 5

Discussion and conclusion

Experiments on coal-biomass blends show that both permeability and porosity decrease with an increase in applied stress. As void space reduces due to compaction from the application of an increased stress the flow paths constrict and permeability reduces (David, Wong, Zhu, & Zhang, 1994) (Zhu, Montesi, & Wong, April 1997). In addition to changes in permeability observed due to porosity reduction, and in the absence of grain breakage, the 100% biomass blends display permeability values an order of magnitude greater than the coal and coal-biomass blends. The particle size of the corn stover and corn stover pellets are distinctively larger than the coal particles. The differing form of the particle shapes and sizes are shown in the Appendix B. The coal particles are difficult to view under the microscope due to the agglomeration of particles (Yu, Standish, & Lu, February 1995). The shape of coal particles is not exactly spherical and varies greatly (Mathews, Eser, Hatcher, & Scaroni, 2007). The coal blends have a greater proportion of finer particles. There is an absence of fines in the corn stover pellets. The permeability is controlled by the finer particles as the finer particles occupy more of the void and thereby decrease porosity (Crawford, Myers, Woronow, Faulkner, & Rutter, October 2002) (Marshall, 1958) (Muecke, February 1979). This explains why the permeabilities of the coal-biomass blends are closer to the permeabilities of coal blends rather than those of the biomass blends.

Raw coals do not have a rigid pore structure but behave as a colloidal gel with water as the solvent. (Deevi & Suuberg, 1987) (Suuberg, Otake, Yun, & Deevi, 1993) Porosimetry studies have shown that porosity dependence with stress is often a complex relation based on various different factors. (Suuberg, Deevi, & Yun, 1995) However for the stress range in this study, the portion where the stress porosity relation is linear is only considered. Considering the similar initial starting porosities for different coal samples the final porosities are same. This indicates that the change in porosity is dependent on the void space available and is independent of the coal properties as particle size of blends is in the same range. This is seen for the stress range in the study and would differ if stress is increased as the void space reduces.

The ultra dense-phase transport of feed operates at very low void fractions - usually below 60%. In this the coal particles are pulverized to a fine standard grind of 70 wt% passing the 200 mesh screen and at a moisture content below 18wt%. Coal grindability is a complex property based on hardness, strength, tenacity and fracture which is measured by the Hardgrove Grindability Index. (Rubiera, Arenillas, Fuente, Miles, & Pis, 1995) Hardgrove Grindability Index is a relative determination of grindability or ease of pulverization of coals when compared to a certain standard. (Hardgrove, 1932) The heterogeneous nature of coal with regards to maturity, petrological constituents, mineral impurities, moisture content along with mechanism of comminution leads to difficulties in reproducibility and repeatability of Hardgrove Grindability Index. (Sengupta, 2002) Coal grinding is done to get ideal particle size as scrubbers and slag formation is dependent on particle size. (Austin & Luckie, 1984) A ball mill is used to reduce coal to

200 mesh. Microstructure of coal greatly influences its strength or resistance to fracture. (Callcott & Smith, 1981) (Schönert, 1972) Effects of pores, microstructure and mineral inclusions play an important part in formation of particles after grinding. (Lytle, Daniel, & Prisbrey, 1983) Particles exposed to individual breakage events are typically angular and irregular and as exposed to longer time periods will lead to rounding of particles. (Kaya, Hogg, & Kumar, 2002) For transport of the feed the pressure drop in the pipes determines the flow. The pressure drop is dependent on friction, length of pipe, porosity, fluid velocity, mass flow rates and cross sectional area of the pipe (Aziz & Klinzing, January 1990) (Vásqueza, Sáncheza, Klinzing, & Dhodapkarb, November 2003). Velocity is dependent upon permeability. It is important to know both permeability and porosity of the blends for ideal design of the feed system.

Permeabilities and porosities values of the feed materials used in this study are not verified for actual usage in the gasification system for which the study was performed. It is proprietary design information was not provided for validation of the results. Permeability and porosity models were independently verified by running flow through experiments with water as per equivalent testing standards. The differences reported by both methods were negligible. Permeability and porosity were calculated for all the samples with helium and nitrogen so it was possible to also validate results on the same system with two different permeating fluids. The data fit a model for a cubic dependency with porosity. It is difficult to determine with the limited data presented here if it is valid over a wider range of permeating fluids or blends. The lignite coal and coal-biomass blends deviate the most from the model while the bituminous, subbituminous and

biomass blends fit the data best. This may be due to the size of pores in the coals with lignite coals having larger size pores than subbituminous pores (Gan, Nandi, & Walker, 1972) (Parkash & Chakrabartty, 1986) (Sharkey & McCartney, 1981). During compaction the larger sized pores in lignite coals would become smaller at a rate faster than the pores in the subbituminous and bituminous coals. This would explain the behavior exhibited for the lignite coals in having a exponent higher than 3. Permeability is dependent on many factors other than merely porosity and grain size as used in the model. It does however provide us with a useful tool to map permeability and porosity which are important in any study of flow through porous media. Laboratory observations are made under conditions of controlled stress and uniform strain rate. The model was validated only for nitrogen as the permeating fluid. The hydrostatic conditions which are applied to the sample may not exist in actual applications. With the design of the two conveyer belts feeding fuel to the gasifier in essence there would be shear stress applied on the feed and it being further studied. It is also possible to determine permeability based on the other factor which we assume to be uniform, grain size. A relation to accommodate a change in grain size can also be developed with further study.

References

Amthor, J. E., Mountjoy, E. W., & Machel, H. G. (1994). Regional-Scale Porosity and Permeability Variations in Upper Devonian Leduc Biuldups: Implications for Reservoir Development and Prediction in Carbonates. *Progress in Energy and Combustion 78*.

Aplin, A. C., Yang, Y., & Hansen, S. (April 25 1995). Assessment of Beta, the Compression Coefficient of Mudstones and its Relationship with Detailed Lithology. *Powder Technology 12*.

Austin, L. G., & Luckie, P. T. (1984). Coal Preparation and Comminution. *Progress in Energy and Combustion Science* .

Aziz, Z. B., & Klinzing, G. E. (January 1990). Dense Phase Plug Flow Transfer: The 1-Inch Horizontal Flow. *Powder Technology* .

Bain, R. L. (1993). Electricity from Biomass in the United States: Status and Future Direction. *Bioresource Technology 46.*

Bear, J. (1972). *Dynamics of Fluids in Porous Media.* Dover Publications.

Beenackers, A. A. (1999). Biomass Gasification in Moving Beds, A Review of Europen Technologies. *Renewable Energy 16*.

Berg, R. R. (1970). Method for Determining Permeability from Reservoir Rock Properties. *Gulf Coast Aaaociation of Geological Societies 20*.

Bernabe, Y., Brace, W. F., & Evans, B. (1982). Permeabiltiy, Porosity and Pore Geometry of Hot-Pressed Calcite. *Mechanics of Materials 1*.

Blake, F. C. (1922). The Resistance of Packing to Fluid Flow. *American Institute of chemical Engineers.*

Brace, W. F., Walsh, J. B., & Frangos, W. T. (March 15 1968). Permeability of Granite under High Pressure. *Journal of Geophysical Research 73*.

Brantley, S. L. (1992). The Effect of Fluid Chemistry on Quartz Microcrack Lifetimes. *Earth and Planetary Science Letters 113*.

Bridgewater, A. V. (July 26 1994). The techincal and economic feasibility of biomass gasification for power generation. *Fuel 74*.

Brown, P. W. (1991). Porosity/ Permeability Relationships. *Materials Scinece of Concrete II.*

Burge, H. L., Roberts, R. W., & Zettle, E. V. (1964). Dense Phase Transport of Powdered Metals for a Tripropellant Rocket System. *Chemical Engineering Progress.*

Burland, J. B. (1990). On the Compressibility and Shear Strength of Natural Clays. *Geotechnique 40*.

Callcott, T. G., & Smith, G. B. (1981). Mechanical Properties of Coal. *Chemistry of Coal Utilization* .

Carman, P. C. (1956). Flow of Gases through Porous Media. *Butterworths.*

Carman, P. C. (1937). Fluid Flow through Granular Beds. *Institution of Chemical Engineers.*

Carman, P. C. (1939). Permeability of Saturated Sands, Soils and Clays. *Journal of Agricultural Science.*

Chapius, R. P. (2004). Predicting the Saturated Hydraulic Conductivity of Sand and Gravel using Effective Diameter and Void Ratio. *Canadian Geotechnical Journal 41*.

Chapuis, R. P., & Aubertin, M. (2003). On the use of the Kozeny-Carman Equation to Predict the Hydraulic Conductivity of Soils. *Canadian Geotechincal Journal.*

Chilingar, G. V. (1963). Relationship between Porosity, Permeability and Grain-Size Distribution of Sands and Sandstones. *Developments in Sedimentology 1*.

Chillingar, G. V. (1964). Relationship between Porosity, Permability and Grain Size Distribution of Sands and Sandstones. *Elsevier.*

Combs, L. P., Ubhayakar, S. K., Breese, L. S., Kahn, D. R., & Lee, W. T. (1980). *Coal Hydrogasification Process Development Second Annual Technical Progress Report Government Fiscal Year 1980, Vol. I: Coal Studies.* National Technical Information Service.

Cormos, C.-C., Starr, F., Tzimas, E., & Peteves, S. (June 15 2007). Innovative Concepts for Hydrogen Production Processes based on Coal Gasification with Carbon Dioxide Capture. *International Journal of Hydrogen Energy 33*.

Costa, A. (2006). Peremabiltiy-porosity relationship: A reexamination of Kozeny-Carman equation based on a fractal pore-space geometry assupmtion. *Geophysical Research Letters 33*.

Crawford, B. R., Myers, R. D., Woronow, A., Faulkner, D. R., & Rutter, E. H. (October 2002). Porosity-Permeability Relationships in Clay-Bearing Fault Gouge. *Society of Petroleum Engineers.*

Dasappa, S., Paul, P. J., Mukunda, H. S., Rajan, N. K., Sridhar, G., & Sridhar, H. V. (October 10 2004). Biomass Gasification Technology – A Route to Meet Energy Needs. *Current Science 87*.

David, C., Wong, T.-F., Zhu, W., & Zhang, J. (1994). Laboratory Measurments of Compaction-Induced Permeability Change in Porous Rocks: Implications for the Generation and Maintenance of Pore Pressure Excess in the Crust. *Pure and Applied Geophysics 143*.

Descamps, C., Bouallou, C., & Kanniche, M. (December 12 2006). Efficiency of an Integrated Gasification Combined Cycle (IGCC) Power Plant including Carbon Dioxide Removal. *Energy 32*.

Deevi, S. C., & Suuberg, E. M. (1987). Physical Changes Accompanying Drying of Western US Lignites. *Fuel* .

Dewhurst, D., & Aplin, A. (January 10 1998). Compaction-driven evolution of porosity and peremability. *Journal of Geophysical Research 103*.

Ehrenberg, S. N., & Nadeau, P. H. (2005). Sandstone vs. Carbonate Petroleum Reservoirs: A Global Perspective on Porosity-Depth and Porosity-Permeability Relationships. *American Association of Petroleum Geologists 89*.

(November 23, 2010). *Electric Power Annual with Data for 2009.* US Energy Information Administration.

Friedman, J. (1979). *Development of a Single-Stage, Entrained-Flow, Short-Residence Time Hydrogasifier, Final Report.* National Technical Information Service.

Friedman, M. (1976). Porosity, Permeability and Rock Mechanics- A Review. *American Rock Mechanics Association.*

Fusselman, S. P., Sprouse, K. M., Darby, A. K., Tennant, J., & Stiegel, G. J. (2009). Pratt & Whitney Rocketdyne/ DOE Advanced Single-Stage Gasification Development Program. *Department of Energy.*

Gan, H., Nandi, S. P., & Walker, P. L. (1972). Nature of Porosity in American Coals. *Fuel 51*.

Griffiths, J. C. (1958). Petrography and porosity of the Cow Run Sand, St. Mary's, West Virginia. *Journal of Sedimentary Petrology 28*.

Hardgrove, R. M. (1932). Grindability of Coal. *ASME* .

Hohenstein, W. A., & Wright, L. L. (1994). Biomass Energy Production in the United States: An Overview. *Biomass and Bioenergy 6*.

Holness, M. B., & Graham, C. M. (1991). Equilibrium Dihedral Angles in the Sysytem H20-Co2-NaCl-Calcite and Implications for Fluid Flow during Metamorphism. *Contributions to Mineralogy and Petrology 108*.

Hsieh, P. A., Tracy, J. V., Neuzil, C. E., Bredehoeft, J. D., & Silliman, S. E. (1981). A Transient Laboratory Method for Determining the Hydraulic Properties of 'Tight' Rocks-I. Theory. *International Journal of Rock Mechanics, Mining Science & Geomechanics 18*.

Jones, S. C. (March 1997). A Technique for Faster Pulse-Decay Permeability Maesurement in Tight Rocks. *Formation Evaluation12*.

Kaya, E., Hogg, R., & Kumar, S. R. (2002). Particle Shape Modification in Comminution. *Kona Powder and Particle* .

Klinzing, G. E. (1981). *Gas-Solid Transport.* McGraw-Hill.

Kotyakhov, F. I. (1949). Relationship between Major Physical Parameters of Sandstones. *Oil Economy 12*.

Kozeny, J. S. (1927). Uber Kapillare Leitung des Wassers im Boden.

Libbin, J. D., & Boehlje, M. D. (February, 1977). Interregional Structure of the U.S. Coal Economy. *American Journal of Agricultural Economics 59*.

Liu, J., Chen, Z., Elsworth, D., Qu, H. Q., & Chen, D. (2011). Interactions of Multiple Processes during CBM Extraction: A Critical Review. *International Journal of Coal Geology*.

Lytle, J. M., Daniel, J. L., & Prisbrey, K. A. (1983). Effect of microstructure on the size and shape of coal particles during comminution. *Fuel* .

Marshall, T. J. (1958). A Relation between Permeability and Size Distribution of Pores. *Journal of Soil Science 9.*

Mathews, J. P., Eser, S., Hatcher, P. G., & Scaroni, A. (2007). The Shape of Pulverized Bituminous Vitrnite Coal Particles . *KONA* .

Maurstad, O. (September 2005). An Overview of Coal based Intergrated Gasification Combined Cycle (IGCC) Technology. *Massachusetts Institute of Technology.*

Moore, E. S. (1922). *Coal: Its Properties, Analysis, Classification, Geology, Extraction, Uses and Distribution.* John Wiley & Sons, Inc.

Muecke, T. W. (February 1979). Formation Fines and Factors Controlling their Movement in Porous Media. *Journal of Petroleum Technology 31*.

Nelson, P. H. (1994). Permeability-porosity relationships in sedimentary rocks. *Petrophysics.*

Neuzil, C. E., Cooley, C., Silliman, S. E., Bredehoeft, J. D., & Hsieh, P. A. (1981). A Transient Laboratory Method for Determining the Hydraulic Properties of 'Tight' Rocks-II. Application. *International Journal of Rock Mechanics, Mining Science & Geomechanics 18*.

Oberg, C. L., Falk, A. Y., Hood, G. A., & Gray, J. A. (1977). Coal Liquefaction under High-Mass Flux and Short-Residence Time Conditions. *American Chemistry Society.*

Oberg, C. L., Falk, A. Y., Kahn, D. R., & Combs, L. P. (1982). *Partial Liquefaction of Coal by Flash Hydropyrolysis, Final Technical Report.* National Technical Information Service.

Olgaard, D. L., & Fitz Gerald, J. D. (1993). Evolution of Pore Microstructures during Healing of Grain Boundaries in Synthetic Calcite Rocks. *Contributions to Mineralogy and Petrology 115*.

Olson, R. E., & Gholamreza, M. (1970). Mechanisms Controlling Compressibility of Clays. *Journal of the Soil Mechanics and Foundations Division*.

Ovesen, C. V., Clausen, B. S., S, H. B., Steffensen, G., Askgaard, T., Chorkendorff, J. K., et al. (1996). A microkinetic Analysis of the Water-Gas Shift Reaction under Industrial Conditions . *Journal of Catalysis 158*.

Parkash, S., & Chakrabartty, S. K. (1986). Microporosity in Alberta Plains Coals. *International Journal of Coal Geology 6*.

Pronske, K., Trowsdale, L., Macadam, S., Viteri, F. '., Bevc, F., & Horazak, D. (May 8-11 2006). An Overview of Turbine and Combustor Development for Coal-Based Oxy-Syngas Systems. *ASME Turbo Expo 2006: Power for Land, Sea and Air*.

Rodrigues, C. F., & Lemos de Sousa, M. J. (2002). Measurement of Coal Porosity with Different Gases. *International Journal of Coal Geology 48*.

Rubiera, F., Arenillas, A., Fuente, E., Miles, N., & Pis, J. J. (1995). Effect of the Grinding Behaviour of Coal Blends on Coal Utilization for Combustion. *Powder Technology* .

Samarasinghe, A. M., Huang, Y. H., & Drnevich, V. P. (1982). Permeability and Consolidation of Normally Consolidated Soils. *Journal of the Geotechnical Engineering Division 108*.

Sandy, C. W., Daubert, T. E., & Jones, J. H. (1970). Vertical Dense-Phase Gas-Solids Transport. *Chemical Engineering Progress Symposium Series.*

Schilling, H. D., Bonn, B., & Krass, U. (1981). *Coal Gasification: Existing Processes & New Developments.* Graham & Trotman.

Schönert, K. (1972). Role of Fracture Physics in Understanding Comminution Phenomena. *Society of Mining Engineers* .

Schutjens, P., Hanssen, T. H., Hettema, M., Merour, J., de Bree, J., & Coremans, J. (2001). Compaction-Induced Porosity/ Permeability Reduction in Sandstone Reservoirs: Data and model for Elasticity-Dominated Deformation. *Society of Petroleum Engineers.*

Sengupta, A. N. (2002). An Assessment of Grindability Index of Coal. *Fuel Processing Technology* .

Sharkey, A. G., & McCartney, J. T. (1981). Physical Properties of Coal and Its Products.

Shiping, L., Yushou, L., Yi, L., Zhenye, W., & Gang, Z. (1994). Permeability-Strain Equations corresponding to the Complete Stress-Strain Path of Yinzhuang Sandstone. *International Journal of Rock Mechanics and Mining Sciences & Geomechanics 31*.

Skempton, A. W. (1970). The Consolidation of Clays by Gravitational Compaction. *Journal of the Geological Society 125*.

Somerton, W. H., & Mathur, A. K. (1976). Effect of Temperature and Stress on Fluid and Storage Capacity of Porous Rocks. *American Rock Mechanics Association.*

Sondreal, E. A., Benson, S. A., Hurley, J. P., Mann, M. D., Pavlish, J. H., Swanson, M. L., et al. (2001). Review of Advances in Combustion Technology and Biomass Cofiring. *Fuel Processing Technology 71*.

Sprouse, K. M., & Matthews, D. R. (June 17 2008). Linear Tractor Dry Coal Extrusion Pump. *Department of Energy.*

Sprouse, K. M., & Schuman, M. D. (November 1983). Dense-Phase Feeding of Pulverized Coal in Uniform Plug Flow. *American Institute of Chemical Engineers 29*.

Sprouse, K., Widman, F., & Darby, A. (March 30 2006). Conceptual Design of an Ultra-Dense Phase Injector and Feed System. *Department of Energy.*

Sprouse, K., Widman, F., & Darby, A. (August 30 2006). Dry Coal Feed System and Multi-Element Injector Test Plan. *Department of Energy.*

Suuberg, E. M., Deevi, S. C., & Yun, Y. S. (1995). Elastic Behavior of Coals studied by Mercury Porosimetry. *Fuel* .

Suuberg, E. M., Otake, Y., Yun, Y., & Deevi, S. C. (1993). Role of Moisture in Coal Structure and the Effects of Drying upon the Accessibility of Coal Structure. *Energy Fuels* .

Tavenas, F., Jean, P., Leblond, P., & Leroueil, S. (September 22 1982). The Permeability of Natural Soft Clays. Part II: Permeability Characteristics. *Canadian Geotechnical Journal 20*.

Tavoulareas, S. E., & Charpentier, J.-P. (July 1995). Clean Coal Technologies for Developing Countires. *The World Bank.*

Taylor, D. W. (1948). *Fundamentals of Soil Mechanics.* Wiley & Sons Inc.

Terzaghi, K. (1925). Principles of Soil Mechanics: III- Determination of Permeability of Clay. *Engineering News-Record.*

Timur, A. (1968). An Investigation of Permeability, Porosity and Residual Water Saturation Relationships. *Society of Petrophysicists and Well Log Analysts.*

Vásqueza, N., Sáncheza, L., Klinzing, G. E., & Dhodapkarb, S. (November 2003). Friction measurement in dense phase plug flow analysis. *Powder Technology* .

Wang, J. A., & Park, H. D. (2002). Fluid Permeability of Sedimentary Rocks in a Complete Stress-Strain Process . *Engineering Geology 63*.

Wang, S., Elsworth, D., & Liu, J. (July 2011). Permeability Evolution in Fractured Coal: The Roles of Fracture Geometry and Water-Content. *International Journal of Coal Geology* .

Wen, C. Y., & Obrien, W. S. (1976). Pneumatic Conveying and Transporting. *Gas-Solids Handling in the Process Industries.*

Xu, P., & Yu, B. (2008). Developing a new form of Permeability and Kozeny-Carman constant for homogenous porous media by means of fractal geometry. *Advances in Water Resources 31*.

Yu, A. B., Standish, N., & Lu, L. (February 1995). Coal Agglomeration and its Effect on Bulk Density. *Powder Technology 82*.

Zeynaly-Andabily, E. M., & Rahman, S. S. (1995). Measurment of Permeability of Tight Rocks. *Measurement of Science and Technology 6*.

Zhang, S., Paterson, M. S., & Cox, S. F. (August 10 1994). Porosity and Permeability Evolution during Hot Isotatic Pressing of Calcite Aggregates. *Journal of Geophysical Research 99*.

Zheng, L., & Furinsky, E. (May 3 2004). Comparison of Shell, Texaco, BGL and KRW Gasifiers as part of IGCC Plant Computer Simulations. *Energy Conversion and Management 46*.

Zhu, W., Montesi, L. G., & Wong, T.-F. (April 1997). Shear-Enhanced Compaction and Permeability Reduction: Triaxial Extension Tests on Porous Sandstone. *Mechanics of Materials 25*.

Appendix A

Photo documentation of sample preparation

Step 1: Two 1” spacers and an end platen are placed in that order onto the end with the piston of the cell. They are covered upto half the end platten with a rubber sleeve. On the top part of the rubber is blue tape.

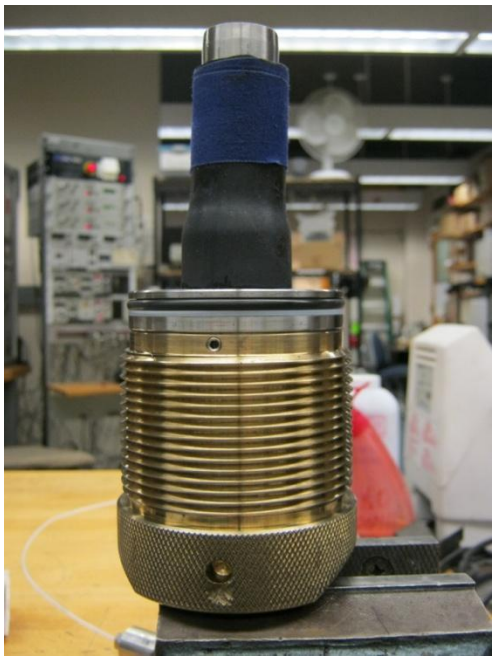

Step 2: A heat shrink tube is cut to a length of 90mm and shrunk around a 1” diameter metal cylinder. After that it is placed on top of the part of the end platen.

Step3: A 2” long sample is created by filling the heat shrink tube with the material to be tested. It is then compacted manually. Another end platen is placed at the top. Frits are placed in between the end platens and the material to ensure none of the gets into the pore pressure lines.

Step 4: Another 90mm heat shrink tube is shrunk around the first one.

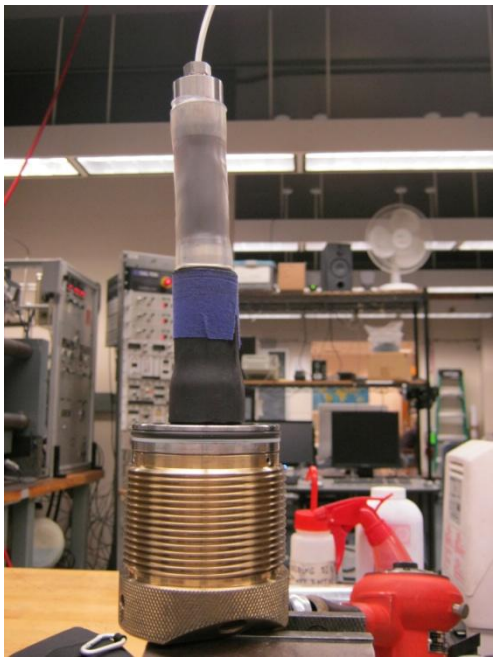

Step 5: An 85mm rubber with a 2” long spacer in it is placed on top of the top end platen. The spacer is placed in such a way as there is in excess of 20 mm of free space at the top. A similar blue tape is used on the rubber as used below.

Step 6: Wire is tied on the two rubbers and also on the heat shrink tubes. The wire is tied on these making sure it is also on the end platens.

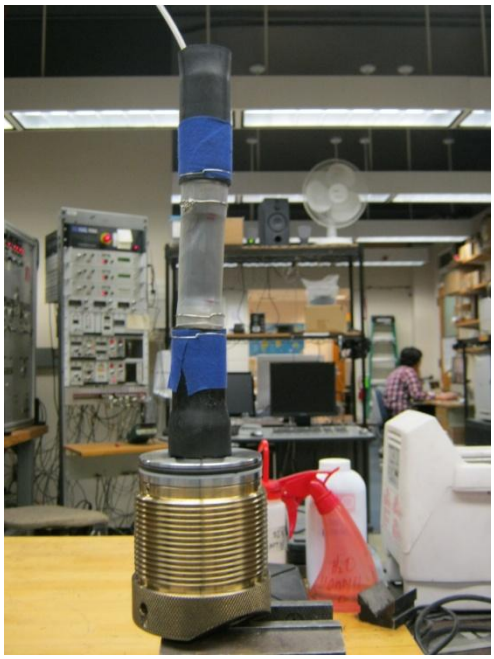

Step 7: Black tape is used to cover the wires.

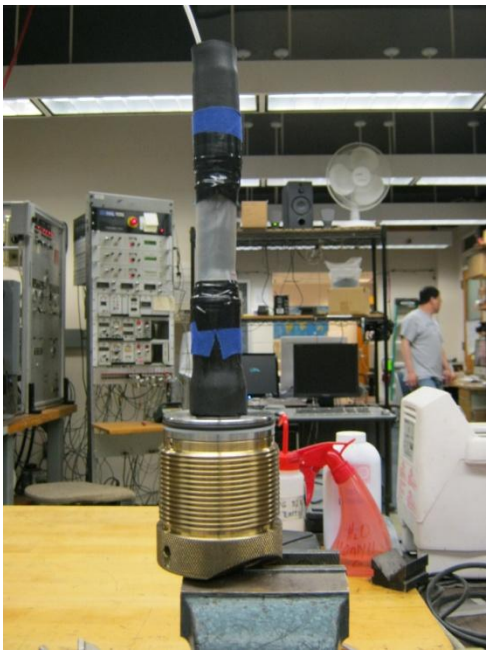

Step 8: A Plastic tube cut along its length is then clamped around the heat shrink tubes.

Step 9: It is then placed in the cell and closed using the other end cap.

Step 10: Axial and confining pressure is applied to the sample in the cell using pumps filled with water. Pore pressure lines carrying gas are connected to reservoirs. Transducers help measure upstream and downstream pressure.

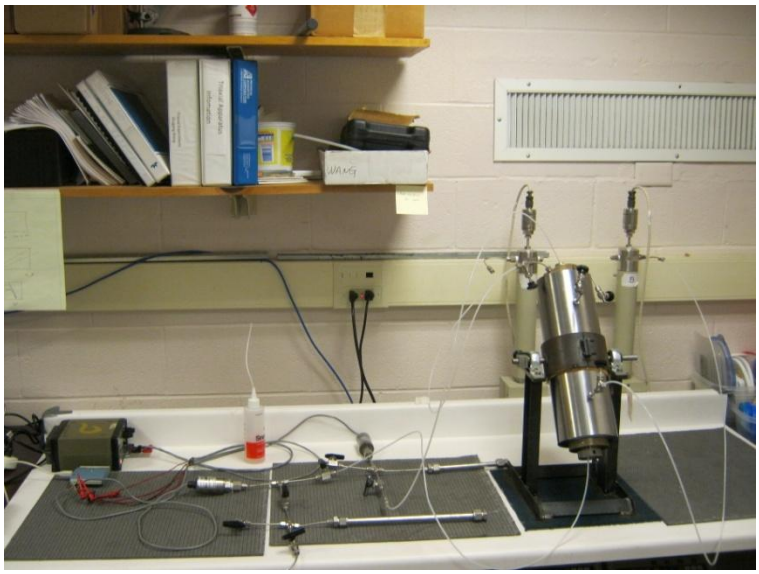

Coal sample inside heat shrink tubing

Appendix B

Micrographs of particles

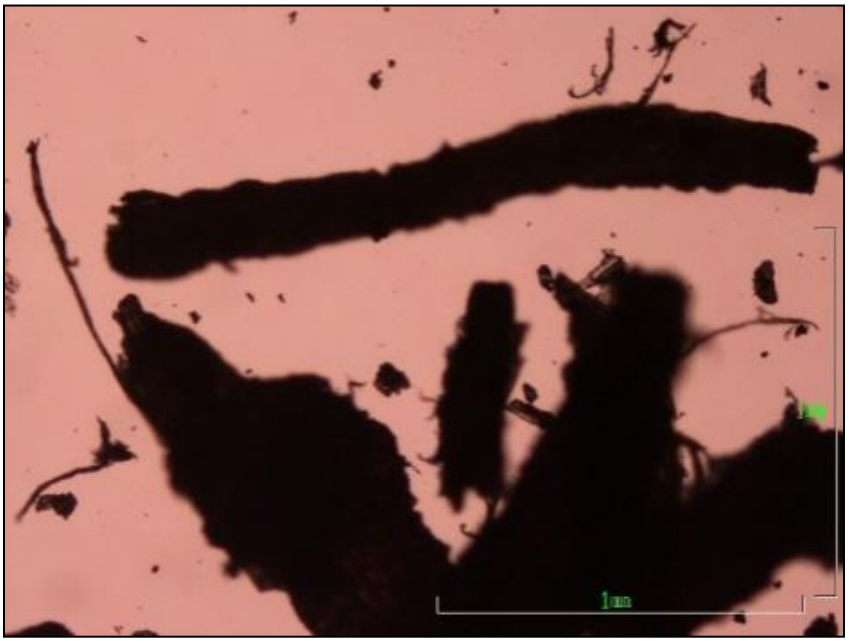

Figure1: Corn Stover

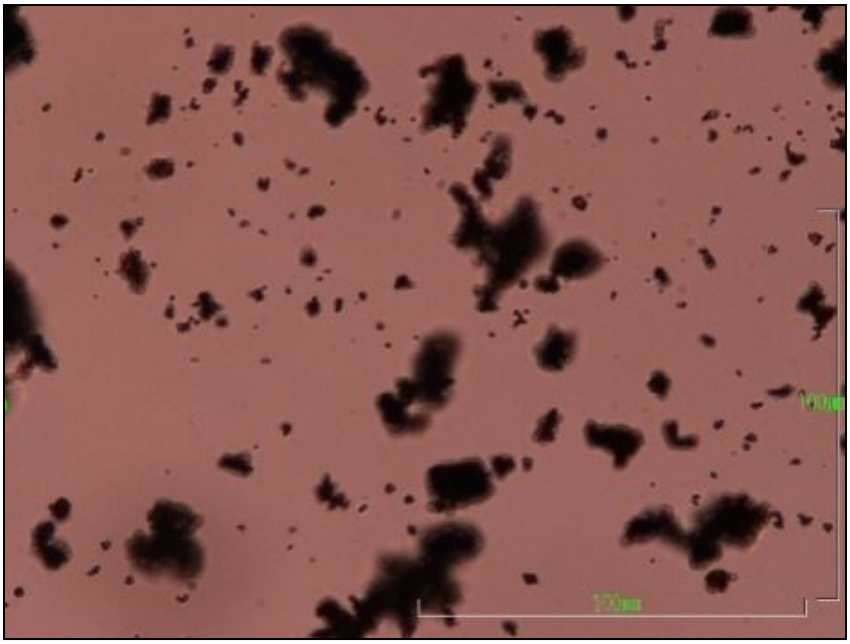

Figure 2: Corn Stover Pellets

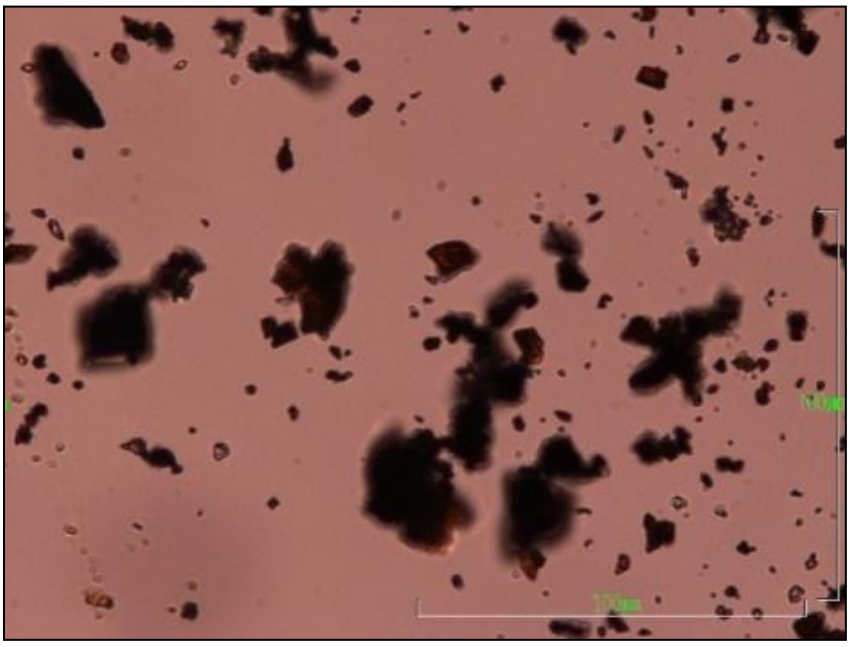

Figure 3: Illinois # 6 Bituminous

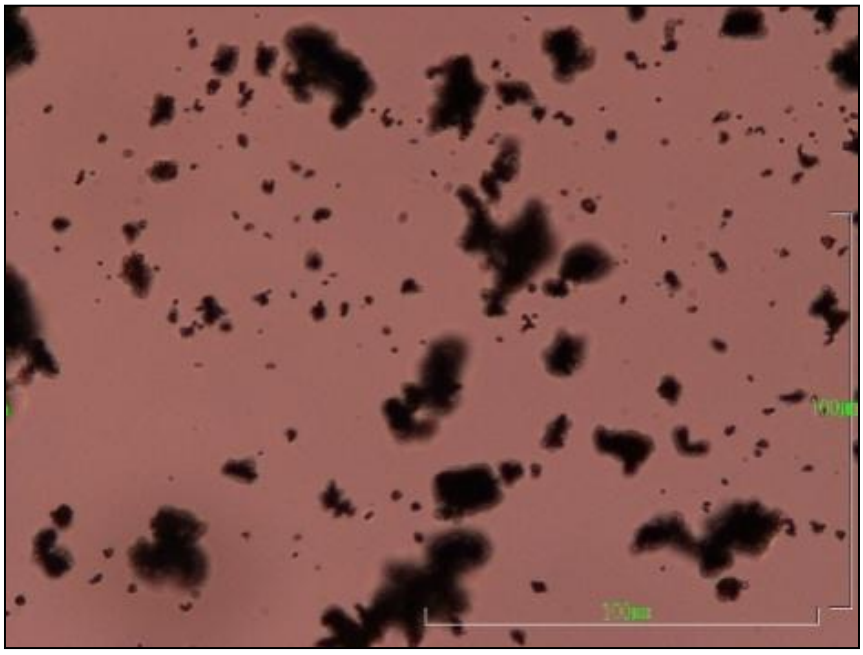

Figure 4: North Dakota Lignite

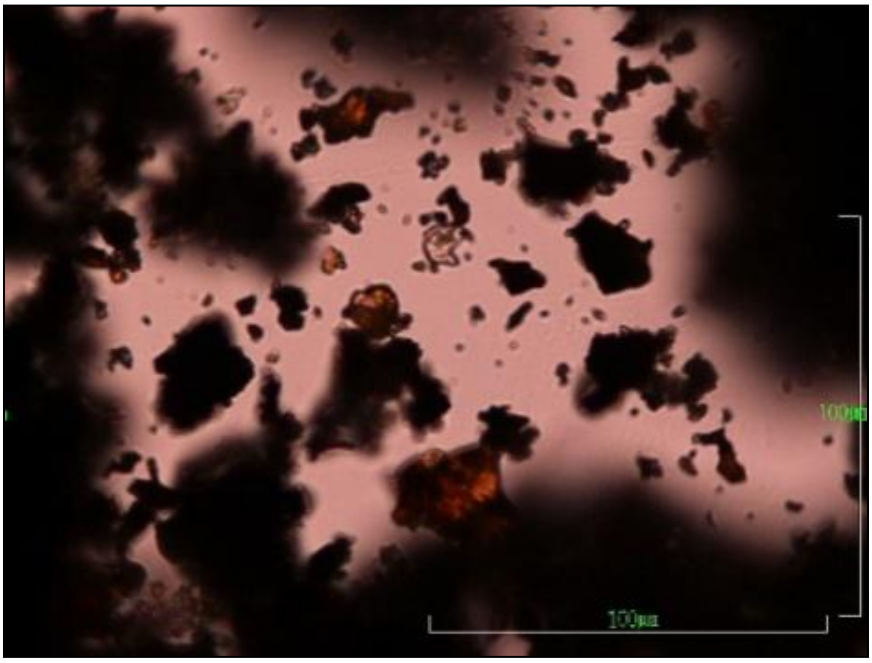

Figure 5: Powder River Basin Subbituminous

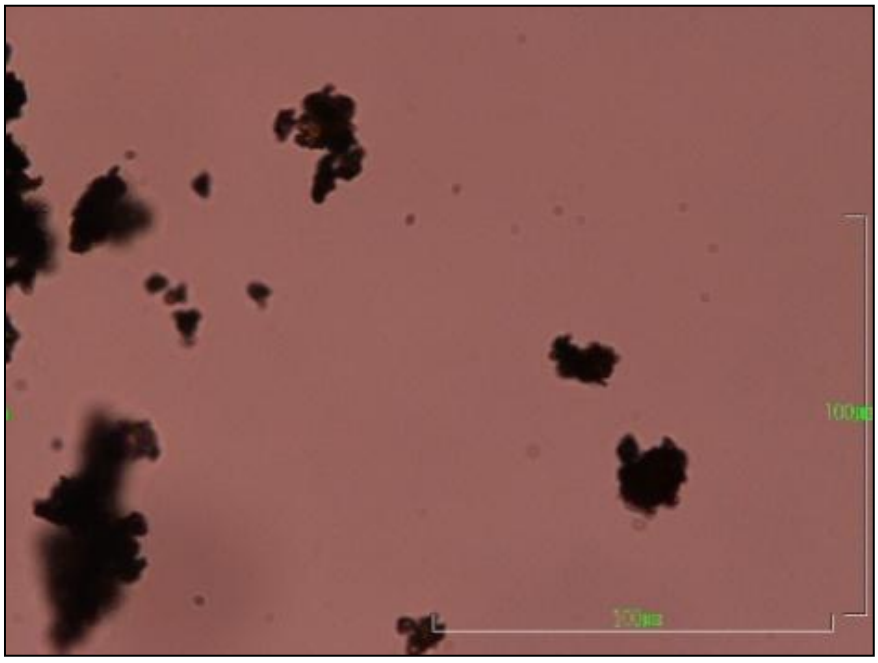

Figure 6: Mississippi Lignite

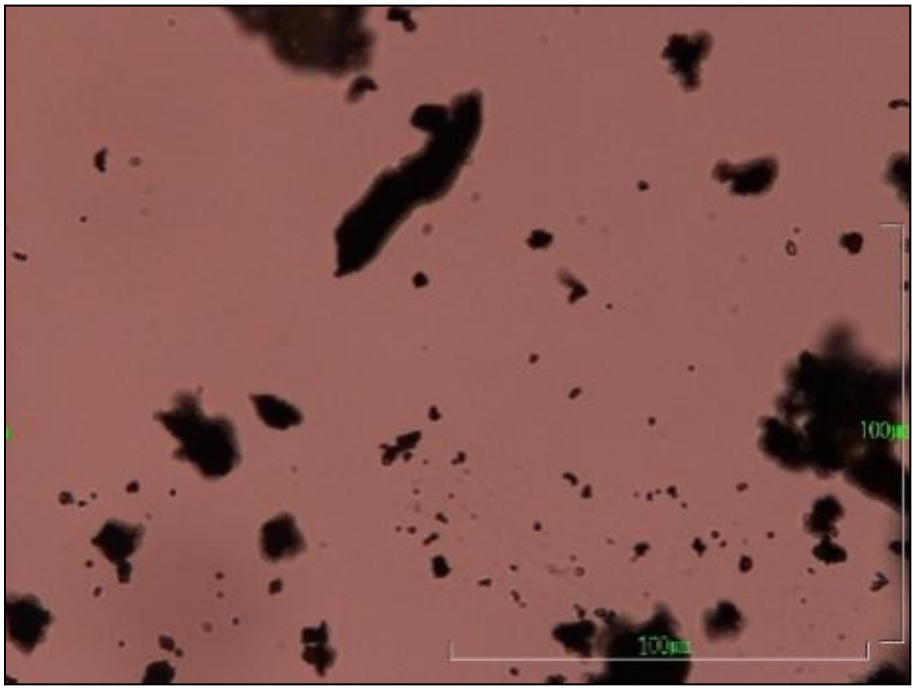

Figure 7: Powder River Basin Transport Subbituminous